

UC San Diego

UC San Diego Previously Published Works

Title

Ancestral roles of the Fam20C family of secreted protein kinases revealed in *C. elegans*

Permalink

<https://escholarship.org/uc/item/9fr7f8tn>

Journal

Journal of Cell Biology, 218(11)

ISSN

0021-9525

Authors

Gerson-Gurwitz, Adina
Worby, Carolyn A
Lee, Kian-Yong
[et al.](#)

Publication Date

2019-11-04


DOI

10.1083/jcb.201807041

Peer reviewed

ARTICLE

Ancestral roles of the Fam20C family of secreted protein kinases revealed in *C. elegans*

Adina Gerson-Gurwitz^{1,2*}, Carolyn A. Worby^{2,3*}, Kian-Yong Lee^{1,2*} , Renat Khaliullin^{1,2}, Jeff Bouffard⁴, Dhanya Cheerambathur^{1,2} , Karen Oegema^{1,2} , Erin J. Cram⁵, Jack E. Dixon^{2,3}, and Arshad Desai^{1,2} 

Fam20C is a secreted protein kinase mutated in Raine syndrome, a human skeletal disorder. In vertebrates, bone and enamel proteins are major Fam20C substrates. However, Fam20C kinases are conserved in invertebrates lacking bone and enamel, suggesting other ancestral functions. We show that FAMK-1, the *Caenorhabditis elegans* Fam20C orthologue, contributes to fertility, embryogenesis, and development. These functions are not fulfilled when FAMK-1 is retained in the early secretory pathway. During embryogenesis, FAMK-1 maintains intercellular partitions and prevents multinucleation; notably, temperature elevation or lowering cortical stiffness reduces requirement for FAMK-1 in these contexts. FAMK-1 is expressed in multiple adult tissues that undergo repeated mechanical strain, and selective expression in the spermatheca restores fertility. Informatic, biochemical, and functional analysis implicate lectins as FAMK-1 substrates. These findings suggest that FAMK-1 phosphorylation of substrates, including lectins, in the late secretory pathway is important in embryonic and tissue contexts where cells are subjected to mechanical strain.

Introduction

The recent discovery of kinases that reside in the secretory pathway and/or are secreted into the extracellular environment has sparked interest in the substrates of these kinases as well as the functional significance of extracellular phosphorylation. One family of secreted kinases, distantly related to the bacterial kinase, HipA, includes Fam20A, Fam20B, Fam20C, Fam198A, Fam198B, and *Drosophila melanogaster* Four-jointed (Tagliabracci et al., 2013; Sreelatha et al., 2015). Originally, these proteins were designated Fams because of shared sequence similarities and lack of information about their functions. These kinases reside in the oxidizing environment of the secretory pathway or outside the cell, and they differ sufficiently from canonical kinases that they were not included in the human “kinome” (Manning et al., 2002). To date, these kinases phosphorylate either protein or sugar substrates. Of these, Fam20C was shown to be the authentic Golgi casein kinase, phosphorylating secreted proteins such as casein and the small integrin-binding ligand N-linked glycoproteins on SerXGlu/pSer (SxE/pS) motifs (Bahl et al., 2008; Zhou et al., 2009; Salvi et al., 2010; Ishikawa et al., 2012; Tagliabracci et al., 2012). These motifs represent the majority of sites identified in secreted phosphoproteomes, and Fam20C was shown to generate the majority of the extracellular

phosphoproteome in liver, breast epithelial, and osteoblast-like cell lines, suggesting roles for Fam20C in a number of different biological processes (Cui et al., 2015; Tagliabracci et al., 2015).

In mammals, Fam20C is most closely related to Fam20A and Fam20B. However, despite considerable sequence conservation, these proteins have very different functions. Fam20A is a pseudokinase that activates Fam20C in specific tissues (Cui et al., 2015). Fam20A forms an extended interaction surface with Fam20C and stimulates its basal kinase activity; a similar interface between two Fam20C molecules is important for basal kinase activity, indicating that a catalytically productive state of Fam20C requires a dimeric configuration with either Fam20A or another molecule of Fam20C (Zhang et al., 2018). Fam20B is not a protein kinase but is a xylose kinase involved in the maturation of proteoglycan chains (Koike et al., 2009; Wen et al., 2014). While vertebrates have all three members of the Fam20 family, invertebrate organisms do not have a gene encoding Fam20A. *D. melanogaster* contains both Fam20C- and Fam20B-like kinases while other invertebrates such as *Caenorhabditis elegans* (nematode), *Ciona intestinalis* (sea squirt), and *Amphimedon queenslandica* (marine sponge) contain only one family member (Fig. 1 A; Tagliabracci et al., 2012). From sequence analysis it was

¹Ludwig Institute for Cancer Research, San Diego Branch, La Jolla, CA; ²Department of Cellular & Molecular Medicine, University of California, San Diego, La Jolla, CA; ³Department of Pharmacology, University of California, San Diego, La Jolla, CA; ⁴Department of Bioengineering, Northeastern University, Boston, MA; ⁵Department of Biology, Northeastern University, Boston, MA.

*A. Gerson-Gurwitz, C.A. Worby, and K.-Y. Lee contributed equally to this paper; Correspondence to Arshad Desai: abdesai@ucsd.edu; Jack E. Dixon: jedixon@ucsd.edu.

© 2019 Gerson-Gurwitz et al. This article is distributed under the terms of an Attribution–Noncommercial–Share Alike–No Mirror Sites license for the first six months after the publication date (see <http://www.rupress.org/terms/>). After six months it is available under a Creative Commons License (Attribution–Noncommercial–Share Alike 4.0 International license, as described at <https://creativecommons.org/licenses/by-nc-sa/4.0/>).

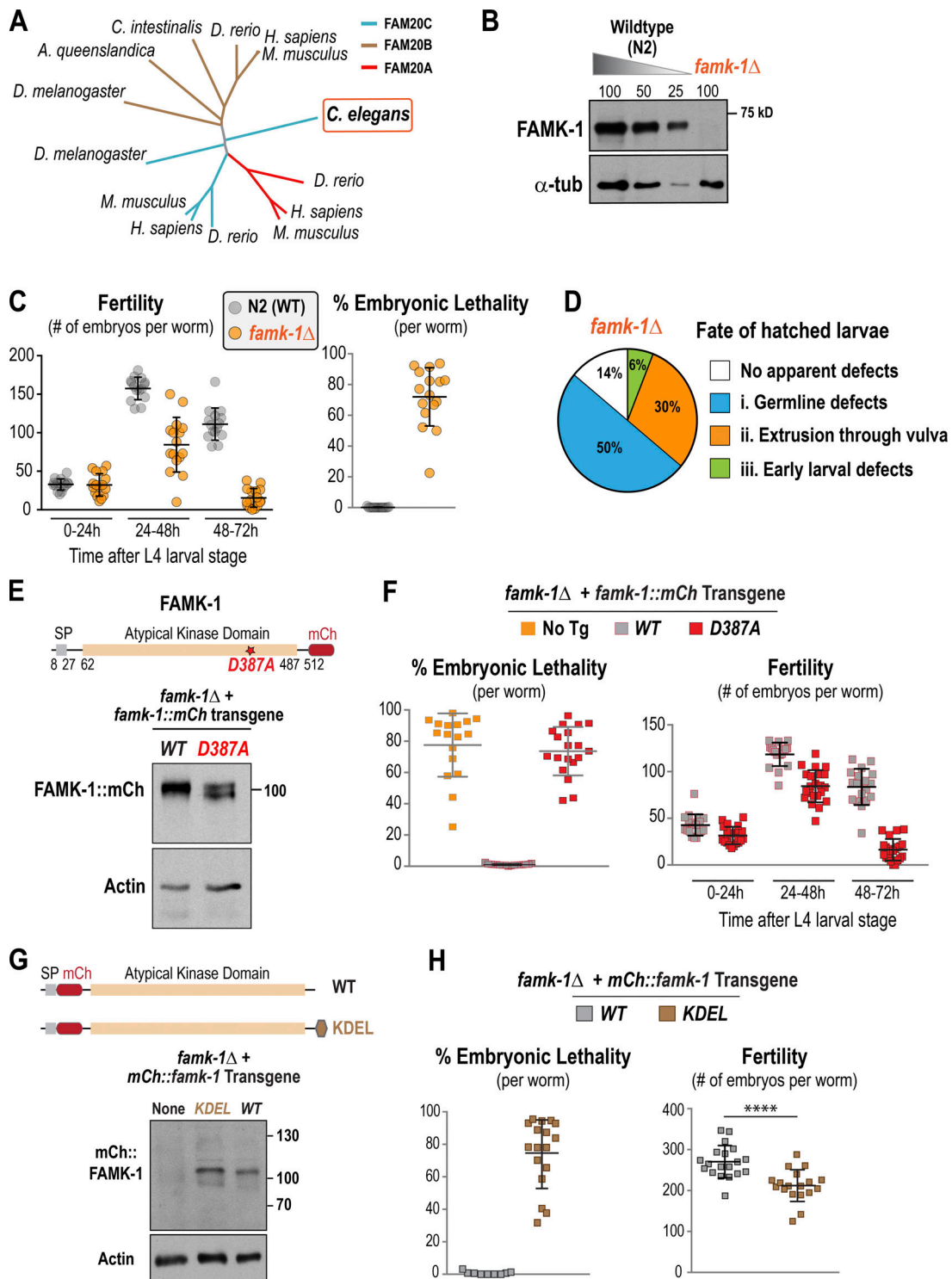


Figure 1. **FAMK-1 catalytic activity and presence in the late secretory pathway contributes to fertility, embryogenesis, and posthatching development.** (A) Phylogenetic tree of Fam20 family kinases. (B) Immunoblot of WT (N2) extract and extract prepared from *famk-1Δ* worms. α -Tubulin serves as a loading control. (C) Fertility and embryonic lethality analysis of individual worms of the indicated genotypes. (D) Phenotypes of posthatching *famk-1Δ* larvae. See also Fig. S1 B. (E) Immunoblot of WT and D387A mutant FAMK-1::mCherry expressed from single-copy transgene insertions. The blot was probed using an anti-FAMK-1 antibody. Actin serves as a loading control. (F) Fertility and embryonic lethality analysis for the indicated conditions. (G) Top: Schematics of WT and KDEL MCh::FAMK-1 (with mCherry inserted after signal peptide [SP]). Bottom: Immunoblot of extracts prepared from the indicated strains probed using an anti-FAMK-1 antibody. Actin serves as a loading control. (H) Fertility and embryonic lethality analysis for the indicated conditions. Error bars are the SD; *****, $P < 0.0001$ (t test).

initially unclear whether *C. elegans* Fam20 had C-like and/or B-like activity (Xiao et al., 2013). Kinase assays using a Fam20C-specific peptide or Fam20B-specific tetrasaccharide demonstrated that *C. elegans* Fam20 functions as a protein kinase and requires the same dimeric interface as human Fam20C for kinase activity (Xiao et al., 2013; Zhang et al., 2018).

In humans, mutations in Fam20C cause a spectrum of defects, collectively named Raine Syndrome, that include generalized osteosclerosis, ectopic calcifications, and malformed cranium/ facial features and usually result in death shortly after birth (Raine et al., 1989). Patients with less severe Fam20C mutations present with hypophosphatemia, ectopic calcifications and dental anomalies (Fradin et al., 2011; Koob et al., 2011). The role of human Fam20C in the regulation of biomineralization-related processes raises the question as to the roles of the Fam20C orthologue in *C. elegans*, an organism with no bones or enamel, and suggests the potential of studying its function in this organism to uncover new roles for this conserved kinase family.

Here, we report the functional characterization of *C. elegans* Fam20C, henceforth referred to as FAMK-1 (FAM20-like kinase 1). Our results reveal a role for FAMK-1 in fertility and embryonic development and demonstrate that C-type lectins are substrates of FAMK-1. In addition, the profile of FAMK-1 expression and analysis of its embryogenesis and fertility requirement suggest that FAMK-1 phosphorylation may be important in tissues subject to repeated mechanical strain.

Results

FAMK-1 contributes to fertility and development of *C. elegans*

A single *C. elegans* gene, *H03A11.1*, encodes a Fam20-related protein that is analogous to Fam20C (Fig. 1 A; Xiao et al., 2013). We have named this gene FAMK-1. Using CRISPR/Cas9, we engineered a deletion of *famk-1* that removes the majority of the ORF (starting from aa 13) and the first 100 bp of the 3' UTR, leading to loss of the gene product (Figs. 1 B and S1 A). *famk-1Δ* mutants exhibit reduced fertility and significant embryonic lethality (Fig. 1 C). Embryos that hatch into larvae exhibited a diverse spectrum of phenotypes, including morphological defects in early larval stages, multinucleation and compromised germ cell partitions in adult germlines, and extrusion of the intestine through the vulva (Figs. 1 D and S1 B). Thus, deletion of *famk-1* is associated with a spectrum of phenotypes, including a significant reduction in fertility and embryonic viability.

To confirm that the phenotypes observed were due to loss of *famk-1* and to test the role of FAMK-1 kinase activity, we replaced endogenous FAMK-1 with transgene-encoded WT or kinase-defective versions of FAMK-1. The FAMK-1 crystal structure and biochemical analysis identified D387 (which is homologous to D478 in human Fam20C) as being critical for kinase activity (Xiao et al., 2013). We engineered a single-copy transgene insertion system to express *famk-1* or *famk-1(D387A)* under control of endogenous *famk-1* promoter and 3' UTR sequences; the transgenes also include the coding region for mCherry fused to the C-terminus (Figs. 1 E and S1 C). Immunoblotting verified that FAMK-1::mCherry and FAMK-1(D387A)::mCherry were equally

expressed (Fig. 1 E). *famk-1::mCherry* fully rescued the embryonic lethality and fertility defects observed in *famk-1Δ*. By contrast, kinase-defective *famk-1(D387A)::mCherry* exhibited embryonic lethality comparable to *famk-1Δ* (Fig. 1 F). *famk-1(D387A)::mCherry* also exhibited a decline in fertility over time after hatching (Fig. 1 F) and similar early larval phenotypes as *famk-1Δ* (not shown). We conclude that the activity of the secreted kinase FAMK-1 contributes significantly to fertility, embryo viability, and development in *C. elegans*.

Retaining FAMK-1 in the ER phenocopies loss of FAMK-1

Fam20 kinases have a signal peptide that directs their entry into the secretory pathway. In human cells, Fam20C concentrates in the Golgi and is also secreted into the extracellular environment (Tagliabracci et al., 2012). It is debated whether Fam20 kinases target substrates throughout the secretory pathway and/or extracellularly (Pulvirenti et al., 2008; Tagliabracci et al., 2015). The embryonic viability and fertility phenotypes of *famk-1Δ* motivated us to test whether presence in the secretory pathway was sufficient for FAMK-1 function. For this purpose, we fused the ER retention signal KDEL to the FAMK-1 C-terminus (Figs. 1 G and S1 D) using *famk-1* transgenes in which mCherry was fused after the signal peptide. The short peptide motif KDEL (Lys-Asp-Glu-Leu) triggers retrograde transport of cargo from the Golgi to the ER, causing proteins bearing it to be retained in the ER (Pulvirenti et al., 2008; Cancino et al., 2014). Immunoblotting confirmed that FAMK-1-KDEL was expressed at comparable levels to WT FAMK-1 (Fig. 1 G). However, in contrast to WT FAMK-1, FAMK-1-KDEL failed to rescue the embryonic lethality or fertility defects of *famk-1Δ* (Fig. 1 H) and exhibited other defects similar to *famk-1Δ* (not shown). Localization analysis indicated that the KDEL sequence altered FAMK-1 distribution and, when expressed in human cells, secretion into the medium of a FAMK-1-KDEL fusion was significantly reduced (see below). Thus, while expressed at normal levels, FAMK-1-KDEL does not provide the function of FAMK-1, suggesting that FAMK-1 must be present in the late secretory pathway and/or extracellularly to execute its functions.

Embryonic lethality in the absence of FAMK-1 is associated with loss of intercellular partitions

We were intrigued by the embryonic lethality observed in *famk-1Δ*, *famk-1(D387A)*, and *famk-1-KDEL*, as it suggested a new role for secreted protein kinase activity. As a first step, we analyzed the phenotype of *famk-1Δ* embryos that failed to hatch and found that they arrested at multiple stages of embryogenesis, with a significant proportion arresting before the morphogenetic events that elongate and shape the embryo into a larva (Fig. 2 A). Imaging of *famk-1Δ* embryos expressing a plasma membrane targeting GFP fusion (GFP::PH) and a red fluorescent chromosome marker (mCherry::H2b) revealed that ~10% of 16- to 32-cell-stage and ~45% of 32- to 64-cell-stage *famk-1Δ* embryos exhibited multinucleation (Fig. 2 B). In contrast, no multinucleation was observed in >200 control embryos imaged under similar conditions. Time-lapse imaging of *famk-1Δ* embryos showed that multinucleation was caused by detachment/

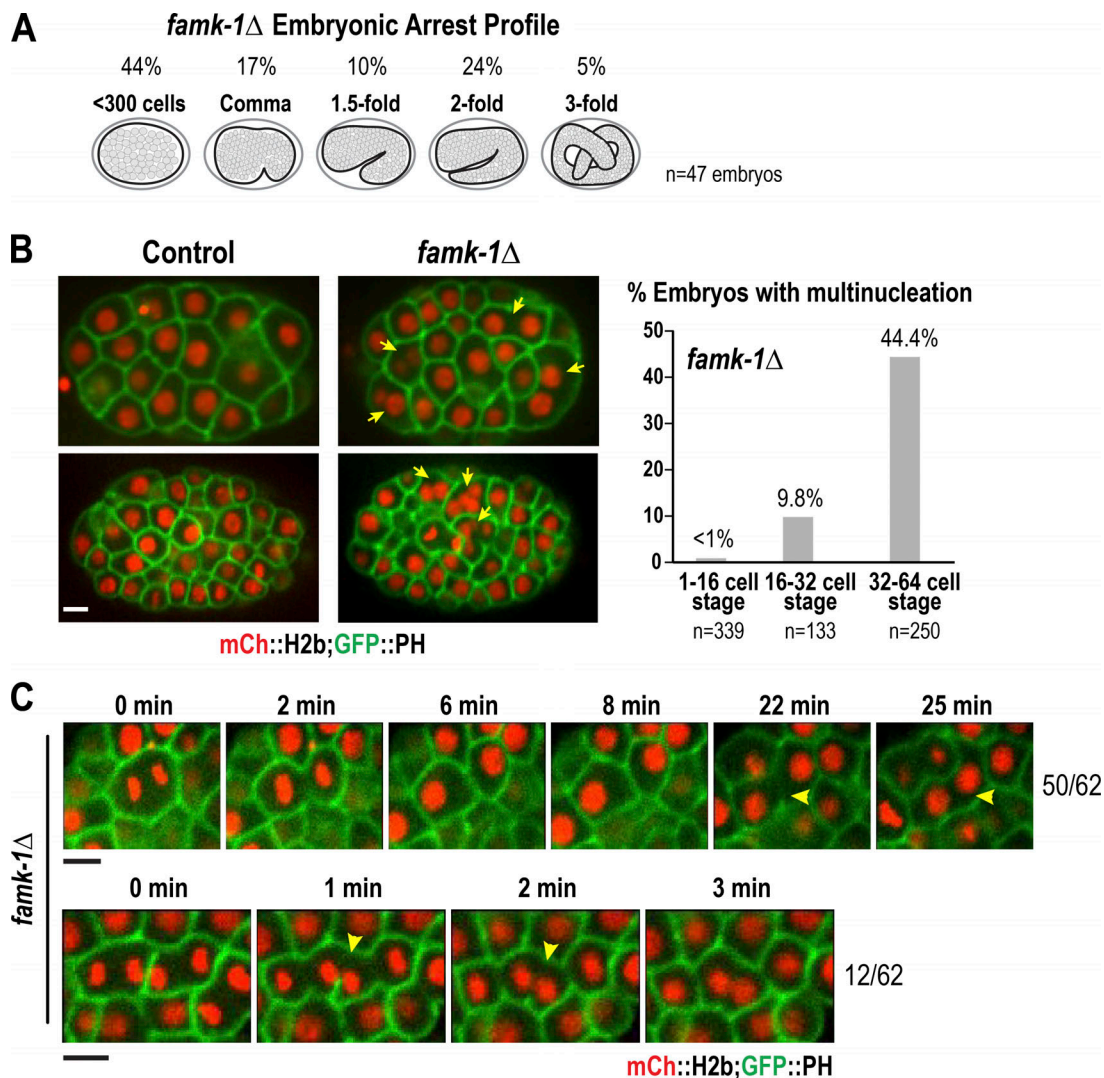


Figure 2. **Loss of cell partitions and multinucleation in *famk-1* Δ embryos.** (A) Arrest stage of *famk-1* Δ embryos that failed to hatch. (B) Images of control and *famk-1* Δ embryos expressing fluorescent probes that label the plasma membrane and chromatin. Arrows indicate multinucleated cells. Scale bar, 5 μ m. The graph on the right shows frequency of embryos with at least one clear multinucleation event at different embryonic stages. (C) High-time-resolution images of *famk-1* Δ embryos. Arrowheads point to partition loss that results in multinucleation; the two classes of events associated with multinucleation and their relative frequency are shown. Scale bars, 10 μ m.

dissociation of the partitions between adjacent cells (Fig. 2 C and Video 1). 50 out of 62 partition-loss events occurred between sister cells (Fig. 2 C, top row) at 16.2 ± 5.4 min (average \pm SD) after full ingress of the cytokinetic furrow. The remainder occurred between cells whose relationship was unclear (Fig. 2 C, bottom row). Multinucleation is often associated with cytokinesis defects. However, multinucleation was rarely observed before the 16-cell stage in *famk-1* Δ embryos (Fig. 2 B), and analysis of furrow ingress in 1-cell embryos revealed no difference from WT (Fig. S2 A), suggesting that general cytokinesis mechanisms are not defective in *famk-1* Δ . The extent of multinucleation in individual embryos was also limited in >24-cell-stage embryos (approximately one to three events were detected per embryo), suggesting that not all partitions formed between cells are unstable in the absence of FAMK-1. Consistent with lack of

general defects in cytokinesis and cell-cell interactions, localization of the major nonmuscle myosin II NMY-2 and the E-cadherin HMR-1 was not noticeably different between WT and *famk-1* Δ embryos throughout embryogenesis (Fig. S2, B and C).

In addition to the early stages of embryonic development, we also monitored *famk-1* Δ embryos at later stages using live imaging of DLG-1::GFP, which marks epidermal cell boundaries (Köppen et al., 2001). Approximately 50% of *famk-1* Δ embryos exhibited epidermal defects, including seam cell defects (mispositioned or aberrant number, 16/33 embryos) and ventral rupture or enclosure defects (7/33 embryos; Fig. S3 A). These epidermal defects may be a consequence of early multinucleation events or may independently contribute to the observed embryonic lethality. We conclude that there is a high frequency of multinucleation in *famk-1* Δ embryos and that this is

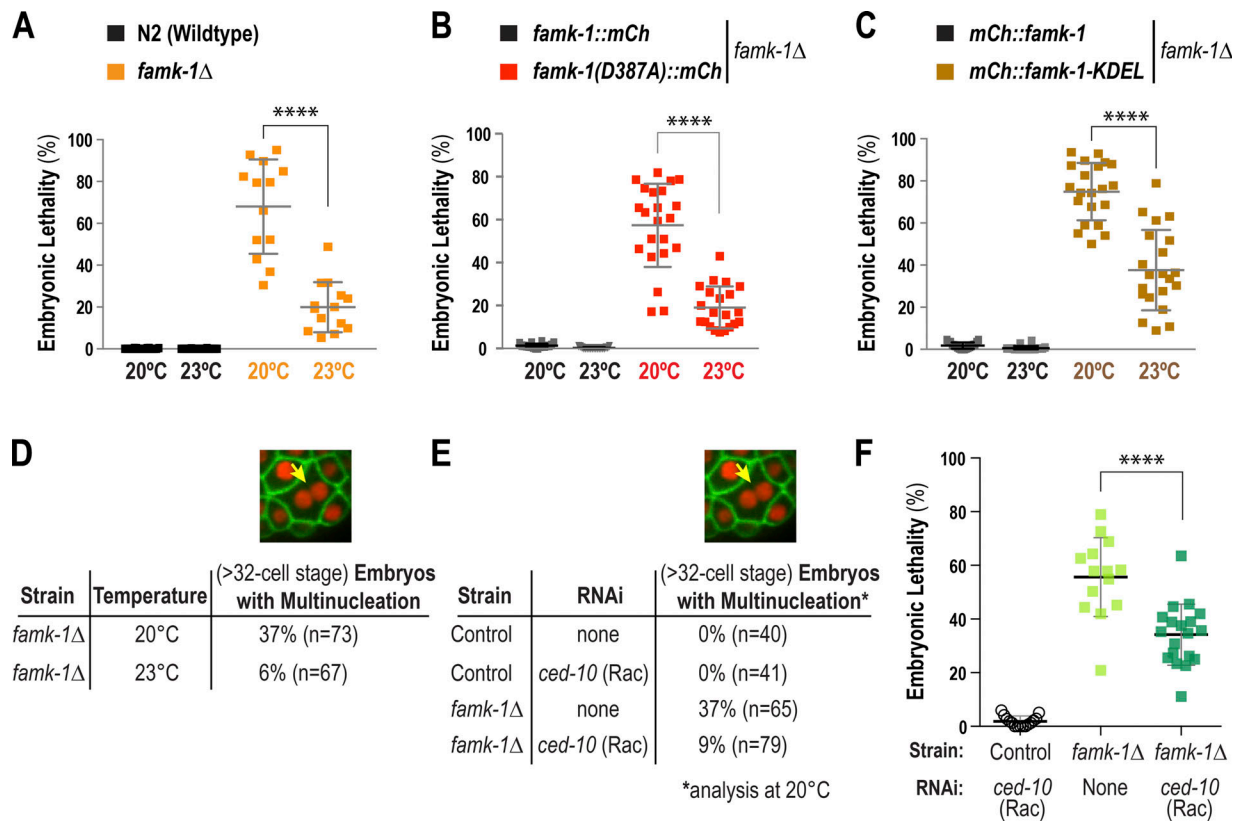


Figure 3. **Increased temperature or reduced cortical tension significantly suppress the embryonic lethality observed in the absence of FAMK-1. (A–C and F)** Embryonic lethality analysis of the indicated conditions. **(D and E)** Analysis for the indicated conditions of multinucleation in embryos that express GFP::PH and mCherry::H2b markers. The strains used for the embryonic lethality analysis in F are the same strains as in D and E. All error bars are the SD; ****, $P < 0.0001$ (t test).

followed by significant morphogenesis defects in later-stage embryos.

The requirement for FAMK-1 during embryogenesis is significantly suppressed by elevated temperature or reduced cortical tension

The above phenotypic analysis of *famk-1Δ* was conducted at 20°C, the temperature at which *C. elegans* is normally propagated. Temperatures >25°C cause sterility in *C. elegans* (Byerly et al., 1976; Petrella, 2014). A typical approach to enhance mutant phenotypes in genetic models is to induce stress by raising the temperature; in *C. elegans*, this is done by placing null mutants at 22–25°C. When conducting such an analysis with *famk-1Δ* embryos, we were surprised to find that elevating the temperature to 23°C significantly suppressed the embryonic lethality of *famk-1Δ* (Fig. 3 A); by contrast, fertility was unaffected (Fig. S3 B). Suppression of embryonic lethality at 23°C was also observed with kinase-defective FAMK-1 (Fig. 3 B) and ER-retained FAMK-1-KDEL (Fig. 3 C). To assess if the temperature increase suppressed the multinucleation phenotype of *famk-1Δ* embryos, we imaged strains with fluorescently marked plasma membrane and chromosomes at 23°C and found that elevated temperature also significantly suppressed multinucleation (Fig. 3 D). Thus, the loss of cell partitions and the embryonic lethality

in the absence of FAMK-1 is suppressed by increasing the temperature.

The effects of temperature on biological systems are complex, but one possibility that may explain the suppression of multinucleation of *famk-1Δ* is that higher temperature makes extracellular interactions between cells more mechanically compliant and less prone to rupture. If this were true, then altering partition stiffness by another means should also suppress the *famk-1Δ* phenotype. To address this possibility, we depleted the major embryonic Rac GTPase, CED-10. Activated Rac directs generation of the Arp2/3-nucleated branched actin network (Pollard, 2007). Consequently, Rac inhibition is associated with reduction of effective cortical viscosity and cortical tension (Gerald et al., 1998; Tseng and Wirtz, 2004). Similar to elevated temperature, Rac/CED-10 depletion suppressed the multinucleation phenotype (Fig. 3 E) and significantly reduced embryonic lethality of *famk-1Δ* (Fig. 3 F).

Collectively, the above results suggest that FAMK-1 phosphorylates substrates that likely act extracellularly to ensure that cells in multicellular embryos robustly maintain their partitions. Whether loss of partitions is due to regression of incomplete cytokinetic abscission or rupture of abscised but adhered cell–cell boundaries is at present unclear. Notably, the contribution of FAMK-1-mediated phosphorylation to integrity of intercellular partitions can be significantly compensated by

increased temperature or by reducing the stiffness of the intracellular actin cortex.

C-type lectins are substrates of FAMK-1

To identify FAMK-1 substrates relevant to its function in embryos, we used an informatics approach based on the fact that FAMK-1, like human Fam20C, targets SxE/pS motifs (Xiao et al., 2013). Notably, Fam20C is predicted to phosphorylate a stretch of serines N-terminal to a double glutamate “EE” motif, as phosphoserine is recognized analogously to a glutamate (Tagliabracci et al., 2015). We therefore searched for gene products with at least three successive FAMK-1 targets (SSSEE). This search yielded 85 hits proteome-wide (Fig. 4 A). Refining this list by predicting if the proteins are secreted or anchored by a transmembrane domain on the cell surface narrowed the number down to 43 (Table S1). Inspection of this protein list revealed that 13 were lectins: 9 C-type lectins and 4 galactoside-binding lectins (Figs. 4 A and S4 A). Notably, the potential target region in these lectins included more than three serines and was followed by a region rich in specific amino acids (H, G, P, and R), suggesting shared origin/regulation.

Lectins are proteins that preferentially bind carbohydrates (Mody et al., 1995; Gorelik et al., 2001; Bies et al., 2004; Minko, 2004) and are classified into subfamilies, including C-type lectins (typically dependent on calcium for carbohydrate binding) and galectins (β -galactoside binding). Both C-type lectins and galectins are found in virtually all organisms. While involved in many biological processes in mammals, including cell-cell and cell-extracellular matrix interactions (Ghazarian et al., 2011), little is known about lectin functions in *C. elegans*. Prior to initiating any genetic analysis, we first tested if FAMK-1 phosphorylated these predicted lectin substrates. We chose 6 of the 13 lectins (5 C-type lectins [CLEC-100, CLEC-104, CLEC-110, CLEC-233, and CLEC-261] and 1 galectin [F46A8.3]) for this analysis. The coding sequence for each lectin was tagged with a V5-His tag and cotransfected with FLAG-tagged WT or D387A kinase-defective FAMK-1 in HEK293 cells. After incubation with radioactive orthophosphate, lectins secreted into the medium were immunopurified and analyzed by immunoblotting and autoradiography (Fig. 4 B). FAMK-1 expression was monitored by preparing cell extracts, immunoprecipitating FAMK-1, and immunoblotting the FLAG tag (Fig. 4 B). To test if the serine stretches preceding the two glutamates were sites for phosphorylation, the glutamates were mutated to alanines and the mutant lectins were cotransfected with WT FAMK-1.

In all six tested lectins, robust phosphorylation was detected in the presence of WT, but not D387A, FAMK-1, indicating that these lectins are phosphorylated by FAMK-1 (Figs. 4, B and C; and Fig. S4 B). With the exception of CLEC-110, all analyzed lectins were secreted into the medium (Fig. 4, B and C; and Fig. S4 B). In addition, the EE>AA mutation significantly reduced phosphorylation of all six tested lectin substrates; the reduction was evident in the autoradiograms and, for CLEC-100, CLEC-104, and CLEC-233, in the reduced mobility shift relative to the WT substrate (Fig. 4, B and C; and Fig. S4 B). For CLEC-233, we additionally compared WT FAMK-1 to FAMK-1-KDEL and observed reduced phosphorylation with the FAMK-1 bearing the

ER retention signal; immunoblotting of the medium confirmed that the KDEL sequence reduced secretion of FAMK-1 (Fig. 4 C).

Collectively, these results indicate that the lectins identified by the informatic analysis are indeed FAMK-1 substrates.

CLEC-233 phosphorylation by FAMK-1 contributes to the embryonic viability and fertility functions of FAMK-1

We next wanted to assess if phosphorylation of lectins contributed to FAMK-1 function in vivo. The very large lectin family in *C. elegans* (numbering >100), of which >10 are likely FAMK-1 substrates (Table S1), makes this a challenging endeavor. While inhibition of individual lectins in genome-wide screens is not associated with phenotypes similar to *famk-1Δ*, inhibition of CLEC-233 was previously reported to lead to mild embryonic lethality (Kamath et al., 2003), leading us to focus on it. CLEC-233 is predicted to be extracellular (Fig. 4 C) and has an extended FAMK-1 target sequence (⁶¹SHSSSSSSSSEE⁷³) and an additional ¹⁹⁰SCE¹⁹² site. From transcriptome analysis, *clec-233* is zygotically expressed at mid-late embryogenesis (Levin et al., 2012), later than when phenotypes are first observed in *famk-1Δ* embryos (*famk-1* mRNA is maternally loaded and likely also zygotically transcribed; Levin et al., 2012); thus, regulation of CLEC-233 is unlikely to account for all phenotypes observed in *famk-1Δ*. To test if CLEC-233 regulation by FAMK-1 has any functional significance, we generated two mutants—a null allele (*clec-233Δ*) and a genome-edited double-glutamate mutant, *clec-233(E72A,E73A)*, which significantly reduces phosphorylation by FAMK-1 in the heterologous expression analysis (Fig. 4 C). When analyzed in a strain background with random transgene insertions expressing fluorescent markers for the plasma membrane and chromatin (strain OD95; Green et al., 2011), *clec-233(E72A,E73A)*, but not *clec-233Δ*, worms exhibited moderately reduced fertility; in addition, a subset of the *clec-233(E72A,E73A)* worms laid a significant proportion of dead embryos (Fig. 4 D). From live imaging analysis, ~13% of *clec-233(E72A,E73A)* embryos (7/54) exhibited multinucleation events (Fig. 4 E); in a small subset of embryos on plates with high embryonic lethality, there was near-complete loss of partitions between groups of cells (Fig. 4 E). Multinucleation and loss of partitions were observed at much later embryonic stages in *clec-233(E72A,E73A)* embryos than in *famk-1Δ* embryos (compare Fig. 4 E to Fig. 2 B), which is consistent with the timing of zygotic transcription of *clec-233* (Levin et al., 2012).

While *clec-233(E72A,E73A)* consistently exhibited embryonic lethality and reduced fertility in the OD95 strain background, it did not exhibit similar phenotypes in a different strain background (strain OD3328), where the plasma membrane and chromatin markers were expressed from a single-copy transgene insertion at a defined site (Fig. S4 C). This dependence on strain background raised the concern as to whether the phenotype in the OD95 strain background was in fact related to presence of CLEC-233(E72A,E73A). We therefore used CRISPR/Cas9 to delete *clec-233(E72A,E73A)* in the OD95 background and generate a “two step-derived” *clec-233Δ*. Removal of *clec-233(E72A,E73A)* suppressed the embryonic lethality and reduced fertility phenotypes (Fig. S4 D). These results suggest that in the OD95 strain background, which is sensitized for germline and

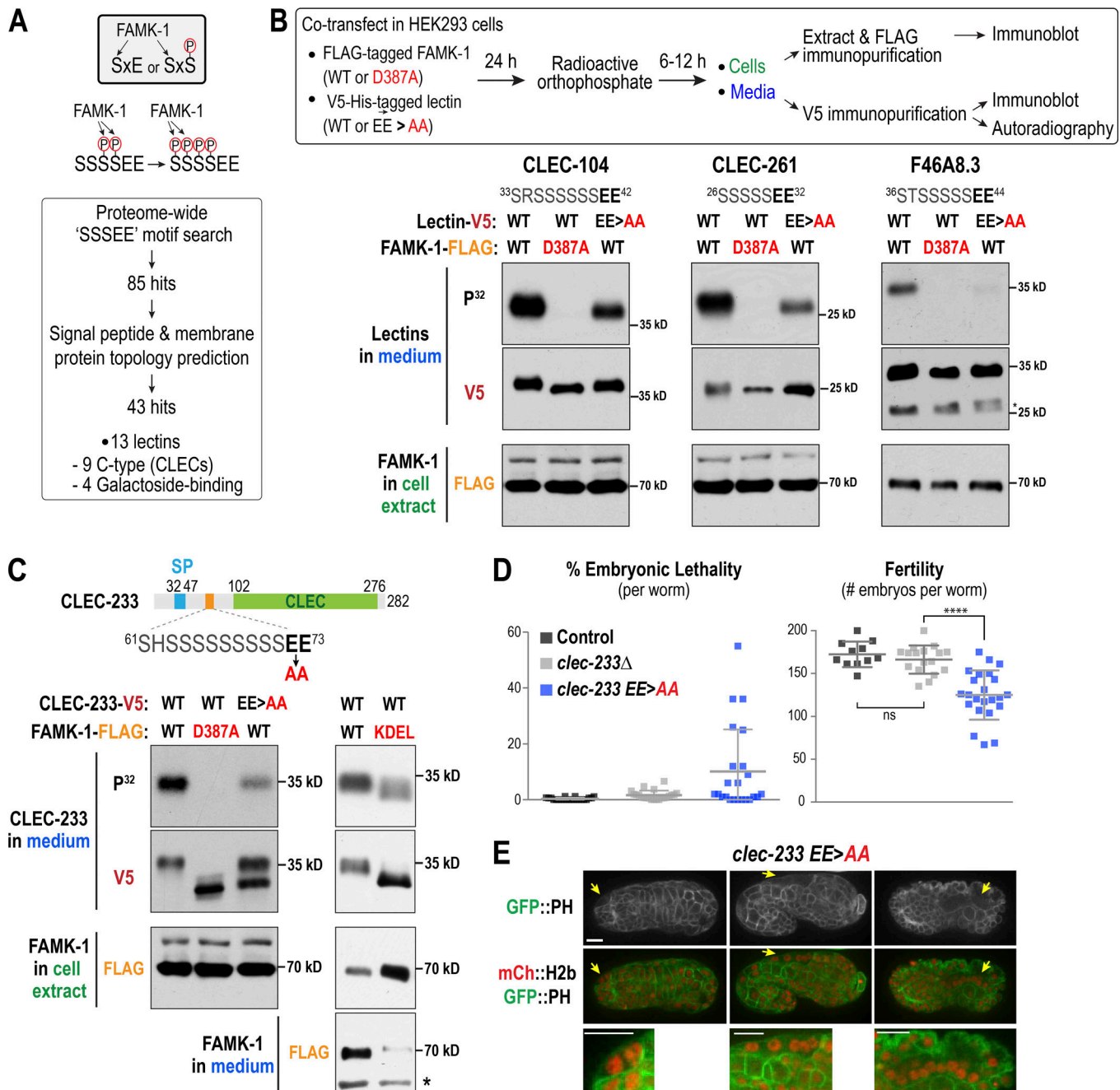


Figure 4. Informatic, biochemical, and functional analysis implicating lectins as FAMK-1 substrates. (A) Schematic highlighting that FAMK-1, which targets serines two residues before a glutamate or a phosphoserine, is predicted to phosphorylate serine clusters preceding two glutamates. The boxed workflow indicates the proteome search approach that identified lectins as potential FAMK-1 substrates. Signal peptide and membrane topology prediction was performed using SPOCTOPUS and SMART. (B) Schematic of experimental protocol employed to test if identified lectins are FAMK-1 substrates. Autoradiograms and blots below show analysis for three candidate lectin substrates; the sequence stretches likely to be targets of phosphorylation are shown above the gels. (C) Analysis of CLEC-233, conducted as in B. KDEL-containing FAMK-1 was also analyzed for its ability to phosphorylate CLEC-233 (panels on the right). (D) Embryonic lethality and fertility analysis for the indicated conditions; note that this analysis was conducted in the presence of transgenes expressing fluorescent fusions that mark the plasma membrane and chromatin (transgenes from strain OD95; Green et al., 2011). Error bars are the SD; ****, $P < 0.0001$ (t test). (E) Images of late-stage embryos genome edited to mutate the two glutamates (*clec-233*(EE>AA)). Arrows point to multinucleation events. Scale bars, 5 μ m.

fertility phenotypes (unpublished data), CLEC-233(E72A,E73A) is more detrimental than the absence of CLEC-233. A potential explanation for this result is that redundancy between the large number of C-type lectins in *C. elegans* can compensate for the

absence of CLEC-233, but not for the presence of its poorly phosphorylated form. The embryos laid by only a subset of *clec-233*(E72A,E73A) worms exhibited significant lethality (Fig. 4 D), suggesting that in the OD95 strain background,

CLEC-233(E72A,E73A) induces an organism-wide defect, potentially in the germline. Consistent with this, worms that laid a high proportion of dead embryos also exhibited the most reduced fertility (not shown) and multinucleation due to compromised germ cell partitions was observed in the germline of adult *clec-233(E72A,E73A)* worms (Fig. S4 E).

While the analysis of CLEC-233 provides some support for lectin phosphorylation contributing to FAMK-1 functions, regulation of CLEC-233 is clearly insufficient to explain the *famk-1Δ* phenotype. This result is not surprising given the large number of potential FAMK-1 substrates, including multiple C-type lectins.

FAMK-1 is prominently expressed in the spermatheca and other tissues in adults

To define the contexts in which FAMK-1 acts beyond embryogenesis, we generated a transcriptional reporter transgene in which the *famk-1* promoter and 3' UTR control expression of a GFP fusion that concentrates in the nucleus (Fig. 5 A). At the L4 larval stage, *famk-1* is transcribed in somatic gonad tissues, prominently in the spermatheca and to a lesser extent in the gonad sheath and vulva, in the body-wall muscles, and in the rectum (Fig. 5 A). *famk-1* expression was also detected in oocytes in the adult gonad (Fig. 5 B). Although transcriptional reporter signal was not detected in embryonic nuclei (not shown), FAMK-1 protein was detected by immunoblotting of embryo extracts (Fig. 5 C).

Localization of mCherry fusions of WT FAMK-1 and FAMK-1-KDEL confirmed FAMK-1 expression in tissues highlighted by the transcription reporter (Fig. S5 A). Notably, the pattern of FAMK-1 localization was consistently different between WT FAMK-1 and FAMK-1-KDEL (Figs. 5 D and S5 A). In the spermatheca and vulva, WT FAMK-1 appeared punctate throughout the organ, whereas FAMK-1-KDEL exhibited a more diffuse localization around nuclei (Figs. 5 D and S5 A). As Fam20C concentrates in the Golgi of human cells (Ishikawa et al., 2012; Tagliabracci et al., 2012), we assessed whether the punctate structures observed in spermatheca represented Golgi. We marked Golgi by expressing an N-terminal fragment (aa 1–144) of α -mannosidase (AMAN-2; Rolls et al., 2002; Paschinger et al., 2006) tagged with mCherry and under control of the spermathecal *sth-1* promoter. Dual-color imaging showed colocalization of FAMK-1 and AMAN-2 in the spermatheca (Fig. S5 B), indicating that the punctate FAMK-1 localization represents its concentration in the Golgi.

In the uterus, WT FAMK-1 was present in the luminal space, but no FAMK-1-KDEL was observed (Fig. 5 D), consistent with it not being secreted. The KDEL fusion revealed FAMK-1 presence in two locations not detected with the transcriptional reporter: the head and a specific cell adjacent to the vulva (potentially the CANL or CANR neuron; Fig. S5 A). These sites may have been missed in the reporter analysis because expression was too low to generate nuclear GFP signal detectable over background autofluorescence. In addition to WT FAMK-1, we also characterized the localization of kinase-defective D387A mutant FAMK-1 (Fig. 1 E). The FAMK-1(D387A) mutant exhibited a similar tissue distribution as WT FAMK-1 (Fig. S5 C).

Taken together, the transcriptional reporter and protein localization analysis indicates FAMK-1 expression in multiple tissues in the adult, which likely underlie the posthatching defects observed in *famk-1Δ* worms.

FAMK-1 expression in the spermatheca is required to maintain spermathecal integrity and fertility

The most prominent localization observed for FAMK-1 in the adult is in the spermatheca, the organ responsible for ovulation and fertilization in *C. elegans* hermaphrodites. The spermatheca is a contractile tube composed of 24 smooth muscle-like cells, separated from the gonad arm by a constriction and from the uterus by a valve (Kimble and Hirsh, 1979; Ward and Carrel, 1979). The spermatheca plays a critical physical role in ovulation by accommodating ovulating oocytes during fertilization and constricting to eject the fertilized oocytes into the uterus. Spermatheca constriction depends on calcium pulses, which occur during the ovulation cycle (Kovacevic et al., 2013). During the first few ovulations in young worms, no reproducible difference in calcium pulses was observed between WT and *famk-1Δ* worms (Fig. S6 A), indicating that there is not a significant defect in the formation of the spermatheca or intercellular signaling in the absence of FAMK-1.

The spermatheca is subjected to repetitive mechanical strain during the reproductively active stage of the animal. While spermathecal structure and function was unaffected in young *famk-1Δ* worms initiating ovulation, the gradual decline in fertility of *famk-1Δ* worms (Fig. 1, C and F) suggested that FAMK-1 expression in the spermatheca was important to maintain its integrity and organismal fertility over time. To test this idea, we expressed FAMK-1 selectively in the spermatheca in the absence of endogenous FAMK-1 by placing *famk-1* under control of the *sth-1* promoter (Bando et al., 2005) and the *famk-1* 3' UTR (Fig. 6 A). GFP::HIS-72 (histone H3.3) expressed under control of these regulatory elements from a single-copy transgene insertion was observed prominently in spermathecal nuclei and two vulval nuclei, but not in any other tissues (Fig. 6 B). As a first step, we imaged WT (N2), *famk-1Δ*, and *famk-1Δ+psth-1::famk-1* worms by differential interference contrast (DIC) over time after the L4 larval stage (Fig. 6 C). We found that spermathecae were abnormally distended or contained oocyte fragments at a significantly higher frequency in *famk-1Δ*, relative to control. The frequency of these defects was significantly reduced by expression of FAMK-1 in spermatheca (Fig. 6 C). Gonad defects were also observed in *famk-1Δ*, and their frequency was also reduced by spermathecal expression of FAMK-1 (not shown). These morphological data suggest that spermathecal expression of FAMK-1 is important to maintain spermatheca integrity over repeated cycles of ovulation and fertilization.

We next assessed the effect of loss of FAMK-1 versus its selective expression in the spermatheca on the fertility of worms. Mating with WT males did not restore fertility of *famk-1Δ* worms, indicating that defective sperm are not the cause of their reduced fertility (Fig. S6 B). Notably, *famk-1* expressed under control of the *sth-1* promoter rescued the fertility defect observed in *famk-1Δ* and also reduced the embryonic lethality of *famk-1Δ* (Fig. 6 D). The eggshell surrounding the embryo forms

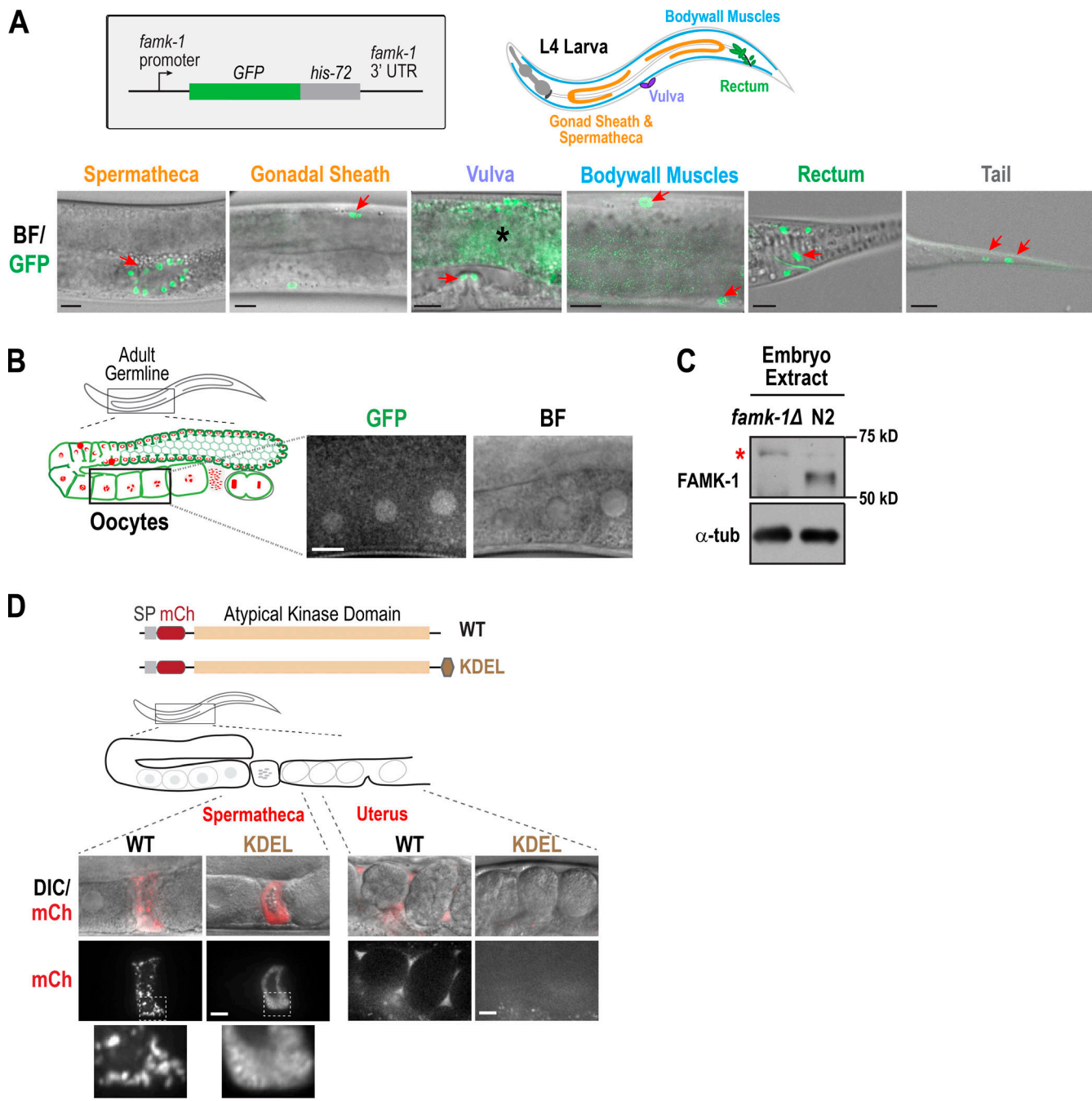


Figure 5. **Tissue distribution of FAMK-1 expression assessed using transcriptional and translational reporters.** (A) Schematic of transcriptional reporter used to analyze expression of *famk-1* in the L4 larval stage. The schematic on the right highlights the tissues where *famk-1* expression was observed. Images below show overlays of bright-field (BF) and nuclear GFP signals; arrows highlight fluorescent nuclei. The most prominent transcription of *famk-1* in the L4 larva (and adult) is in the spermatheca. Asterisk marks background autofluorescence. Scale bars, 10 μ m. (B) Image of oocytes in an adult highlighting *famk-1* expression in the germline. Scale bar, 10 μ m. (C) Immunoblot of embryos purified from the indicated strains. Asterisk marks a background band. α -Tubulin serves as a loading control. (D) Comparison of mCherry-fused WT and KDEL FAMK-1 in the spermatheca and the uterus. For images in other tissues, see Fig. S5. Scale bar, 10 μ m.

after fertilization, which occurs during passage through the spermatheca. Thus, spermatheca-expressed and secreted FAMK-1 may end up in the extracellular space between the embryo plasma membrane and the outer eggshell layers, which could contribute to the reduction in embryonic lethality. The extrusion through vulva phenotype, observed in ~30% of *famk-*

1 Δ worms (Figs. 1 D and S1 B), indicative of loss of vulval integrity (Reinhart et al., 2000; Leiser et al., 2011, 2016), was also rescued by *psth-1*-driven FAMK-1 (0/25 worms analyzed exhibited this phenotype), potentially due to the *sth-1* promoter being active in specific vulval cells (Fig. 6 B). In contrast, morphological defects at early larval stages were observed at a

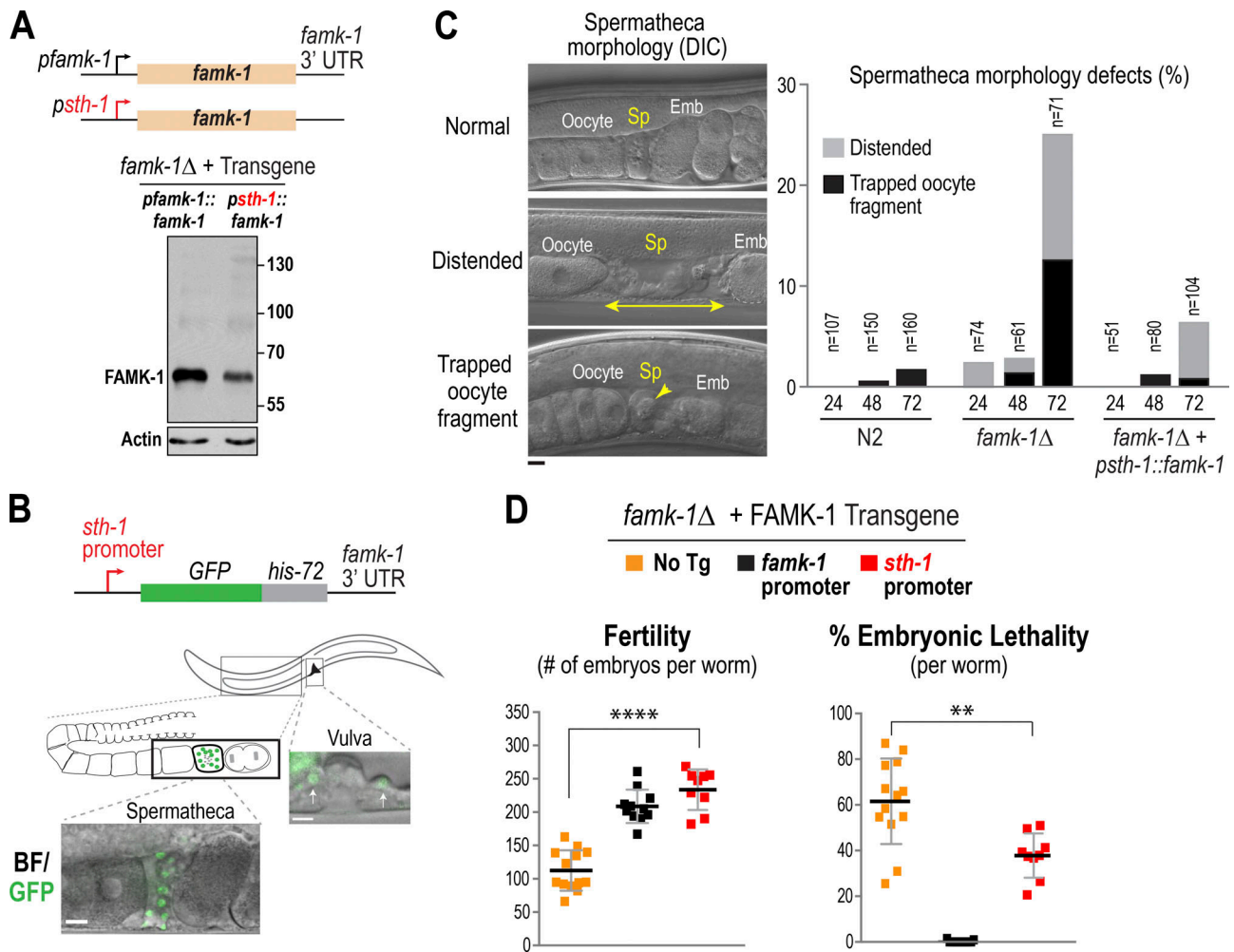


Figure 6. **FAMK-1 expression in the spermatheca maintains spermathecal integrity and organismal fertility.** (A) Immunoblot of the products of the two transgenes schematized above in the absence of endogenous FAMK-1. Actin serves as a loading control. (B) Images of a nuclear GFP reporter expressed under control of the spermathecal promoter *psth-1*. The reporter shows strong expression in the spermatheca and weaker signal in two cells in the vulval region; no additional expression was observed. Scale bar, 10 μ m. (C) Spermatheca morphology analysis for the indicated conditions conducted using DIC imaging. Representative images show a normal, abnormally distended (double arrow), and oocyte fragment (arrowhead)-containing spermatheca. Scale bar, 10 μ m. Graph shows frequency of defective spermatheca for the indicated conditions. (D) Embryonic lethality and fertility analysis for the indicated conditions. ****, $P < 0.0001$; **, $P < 0.01$ (*t* tests).

similar frequency to *famk-1*Δ (not shown). Overexpression of *psth-1*-driven FAMK-1 from extrachromosomal arrays also restored brood size, but embryonic lethality was only mildly reduced (Fig. S6 C). Thus, spermathecal expression of FAMK-1 is sufficient to maintain spermathecal integrity over repeated cycles of mechanical strain and restores the fertility of *famk-1*Δ.

Discussion

New functions for the secreted protein kinase family

The field of secreted kinases originated with the finding that FAM20C encoded a kinase that was sufficiently distinct in primary sequence from canonical kinases to have been left off the kinome tree (Manning et al., 2002; Johnson and Hunter, 2005). Mammalian Fam20C phosphorylates secreted proteins, including a number of calcium-binding proteins, at SxE/pS motifs (Ishikawa et al., 2012; Tagliabracci et al., 2012; Lindberg et al.,

2015). While Fam20C is ubiquitously expressed, it is present at higher levels in mineralized tissues, and mutations in humans result in Raine syndrome, a rare bone dysplasia (Raine et al., 1989; Simpson et al., 2007). Removal of Fam20C in mice results in bone lesions and dental abnormalities, among other phenotypes (Wang et al., 2010; Vogel et al., 2012). Based on these findings, functional analysis of Fam20C in mammals has focused on calcium-binding proteins in mineralized tissues. However, the majority of phosphorylation on SxE/pS motifs in secreted phosphoproteomes is in proteins with no apparent roles in biomineralization (Bahl et al., 2008; Zhou et al., 2009; Carrascal et al., 2010; Salvi et al., 2010). Furthermore, depletion of Fam20C uncovered >100 secreted substrates whose annotations span a broad range of biological processes (Tagliabracci et al., 2015). Thus, Fam20C is likely to act broadly in phosphorylation of extracellular proteins and contribute as-yet-unknown functions.

To address roles of Fam20C not involving biomineralization, we initiated a study of Fam20C in *C. elegans*, an organism that shares a common ancestor with humans ~500–600 million years ago and has no bones or teeth. *C. elegans* has one Fam20C-like predicted protein, FAMK-1, which has been structurally and biochemically characterized to be a protein kinase targeting SxE/pS motifs (Xiao et al., 2013; Zhang et al., 2018). We show that FAMK-1 is important for embryogenesis, fertility, and development of *C. elegans* and that lectins are one substrate class that may contribute to these functions. We also demonstrate the importance of FAMK-1 transit into the late secretory pathway for its functions, document expression of FAMK-1 in multiple tissues, and demonstrate importance of its expression in the spermatheca for fertility. Collectively, our findings lead us to propose that phosphorylation of extracellular substrates by FAMK-1 is important in contexts where tissues undergo repeated mechanical strain. In light of this proposal, it is interesting to note that a link between Fam20C phosphorylation and prevention of cardiac arrhythmia has been reported in humans (Pollak et al., 2017).

FAMK-1 must transit into the late secretory pathway to execute its functions

An important question in the secreted kinase field is where in the secretory pathway phosphorylation of functionally critical substrates occurs. In human cells, fusion of the ER retention signal KDEL to Fam20C did not prevent phosphorylation of selected secreted substrates in tissue culture cells, suggesting that substrate phosphorylation can occur in the lumen of the ER (Tagliabracci et al., 2015). However, whether this extent of phosphorylation is sufficient for Fam20C function is unclear. We found that the ER-retained FAMK-1, while expressed at normal levels, exhibited nearly identical phenotypes as the *famk-1*-null mutant. This result indicates that FAMK-1 activity is functionally critical in the late secretory pathway, specifically in the Golgi and possibly also in the extracellular environment.

Lectins: One class of FAMK-1 substrates

To identify FAMK-1 substrates in an unbiased manner, we used the fact that FAMK-1 phosphorylates proteins within SxE/pS motifs (Tagliabracci et al., 2012), and thus is able to phosphorylate serines preceding two glutamates, to search the *C. elegans* proteome and then conducted biochemical analysis to analyze phosphorylation using heterologous expression. These efforts identified lectins, proteins with carbohydrate-recognition domains, as potential FAMK-1 substrates. Lectin function in *C. elegans* is poorly studied (in part because of the very large expansion of lectins in this organism [there are >200 lectin-encoding genes]; Takeuchi et al., 2008). In mammals, lectins are known to be involved in cell-cell contacts, lipid binding, and the immune response (Ghazarian et al., 2011). Using heterologous expression in human cells, we confirmed that six tested lectins were FAMK-1 substrates and that mutation of the double-glutamate site reduced their phosphorylation. Functional analysis suggested that reducing FAMK-1 phosphorylation of one lectin (CLEC-233) resulted in mild phenotypes in embryos analogous to those observed in *famk-1Δ*. Lectins are increasingly

recognized as critical players in diverse aspects of multicellular life (Brown et al., 2018). In particular, there is growing evidence for potential functions for C-type lectins in bone mineralization and/or mineralized structure formation (Wewer et al., 1994; Mann and Siedler, 2006; Yue et al., 2016). C-type lectins of the mammalian OCIL family inhibit osteoclast formation (Zhou et al., 2002; Nakamura et al., 2007) and resemble *C. elegans* CLEC-233 in that they are composed of an intracellular domain followed by a transmembrane domain and an extracellular C-type lectin-like domain that contains an “SxE” motif (Zhou et al., 2002). Future work will be needed to test if C-type lectins are functionally important Fam20C substrates in mammals.

FAMK-1 expression and phenotypic spectrum: A role for extracellular phosphorylation by FAMK-1 in the function of mechanically strained tissues?

FAMK-1 is expressed in multiple tissues and has a complex phenotypic spectrum, which is consistent with FAMK-1 potentially targeting a diverse set of extracellular substrates in different tissues. Based on its pattern of expression and the phenotypes observed, we propose that one important role of FAMK-1 phosphorylation is to maintain functionality of tissues/organs under repeated mechanical strain. The most prominent expression of FAMK-1 is in the spermatheca, an organ that undergoes repeated cycles of extension and relaxation. While spermathecal structure and early function was normal in the absence of FAMK-1, we show that spermathecal expression of FAMK-1 is important to maintain spermathecal integrity and fertility over time. A second example is the ~30% of adult *famk-1Δ* worms that exhibit extrusion of the intestine through the vulva; the vulva is another organ that undergoes repeated cycles of mechanical strain during egg-laying. Under control of the *sth-1* promoter, *famk-1* was expressed in vulval cells and rescued the extrusion-through-vulva phenotype of *famk-1Δ* worms.

In embryos lacking FAMK-1 activity, the major defect observed was multinucleation; this phenotype was observed at stages when cells are likely under mechanical strain from neighbors. Notably, this phenotype was significantly reduced by either temperature elevation or reduction of intracellular cortical tension. Collectively, these observations lend support to the idea that FAMK-1 phosphorylation of extracellular substrates is important in mechanically strained contexts. Precisely how FAMK-1 phosphorylation acts in these diverse contexts will require future work to elucidate.

In summary, we present here functional analysis of the Fam20C-related secreted kinase FAMK-1 in *C. elegans*, an organism that lacks the structures (bones and teeth) most prominently associated with the function of Fam20C in mammals. Our findings highlight the multiple different contexts in which FAMK-1 acts and demonstrate that it must transit into the late secretory pathway to execute its functions. In addition, our efforts define a new family of secreted substrates for FAMK-1, the lectins. The tools we established should enable future systematic analysis of target substrates and potential functions of their extracellular phosphorylation in all of the different contexts where this secreted kinase is produced.

Materials and methods

C. elegans strains

All strains used in the study are listed in Table S2.

Genome-edited strains

The *famk-1Δ* allele (*famk-1(lt33::cb-unc-119+)*, OD2102) was generated using CRISPR/Cas9. A repair plasmid (pOD2744/pAG58) was used, which contains the *Cb-unc-119* selection marker and *famk-1* locus homology arms. The 5' homology arm is 3,067 bp long, composed of 3,041 bp upstream of the *famk-1* ORF and the first 26 bp of the ORF. The 3' homology arm is 1,687 bp, beginning 190 bp downstream of the *famk-1* stop codon. A mix of two guides was used: 5'-CGATTATTCACCTTGGCGAT-3' (N-terminus) and 5'-TGGATGGGATACCTTCTTG-3' (3' UTR). The knockout strain was genotyped and backcrossed seven times to N2 (WT).

A co-CRISPR strategy (Arribere et al., 2014; Kim et al., 2014) using the *dpy-10* marker was used to generate the *clec-233* null mutant and the *clec-233(E72A,E73A)* mutant allele. A 1:4 mix of *dpy-10/clec-233* CRISPR RNA (crRNA; 100 μM final; Integrated DNA Technologies) was prepared. The *dpy-10* target sequence was 5'-GCTACCATAGGCACCACGAG-3'. For *clec-233* deletion, a mix of two guides was used: 5'-ATGTACGTATGTGGAAAGAG-3' and 5'-GTTTTTTTACAATCCCGGTT-3'. For *clec-233(E72A,E73A)*, the target sequence was 5'-GCTCATCGTCCGAAGAGCA-3'. The crRNA:tracrRNA duplex was generated by 5-min incubation at 95°C followed by 5 min incubation at room temperature. A mix of 2.2 μl crRNA:tracrRNA duplex, 4.8 μl of 40 μM of purified *Streptococcus pyogenes* Cas9-NLS protein (a gift from K. Corbett, University of California, San Diego, La Jolla, CA) and 1 μl (1.2 μg) single-stranded DNA repair template (Valuegene).

To delete *clec-233(E72A,E73A)* for the "two-step-derived" *clec-233Δ* (Fig. S4 D), a mix of two target sequences was used (5'-ATGTACGTATGTGGAAAGAG-3' and 5'-GTTTTTTTACAATCCCGGTT-3').

For *clec-233Δ*, the sequence of the repair template was 5'-**ggtatactactactaacttagacaattacaacaaaaatacgaagtttgataatttatggcatgcttaacgt**TTAACGTGATACCCCTCaccgggattgtaaaaaacagaaaaattggttaac-3', where bold indicates the sequence downstream of *clec-233* ORF (in 3' UTR), capitalized letters represent the sequence at the 3' end of *clec-233* ORF, and underlining represents the sequence ending 7 bp upstream of the *famk-1* ORF (in 5' UTR region).

For *clec-233(E72A,E73A)*, the sequence of the repair template was 5'-GTCTATGTGGTCTATGTGGTGGTCTATGGGGCCTGTGTGCGGTCTATGATGGCCATGCGCTGCGGACGATGAGCTAGACGAAGACGAAGAGTGGGAGTAATAGCCTCCCCACCTCCACCACCT-3' (underlined nucleotides introduce the E72A and E73A mutations).

The final mix was injected into gonads of OD95 gravid adult worms (which carry transgenes expressing GFP::PH(PLC1delta1) and mCherry::HIS-58 markers). Injected worms were singled on plates and maintained at 23°C. 3 d later, F1 progeny were screened and ~40 Roller worms were singled on plates, allowed to lay eggs, and then screened by PCR for presence of *clec-233* deletion or introduction of the point mutations.

For genotyping the *clec-233* deletion, one of two combinations of oligos that distinguish between WT and deletion alleles was

used: combination 1 (forward, 5'-GAGTTCAGAGACCTAATGG-3' [5' UTR]; reverse-1, 5'-AGGAATAGAATAGCAACCCT-3' [ORF]; and reverse-2, 5'-GAGTGAGGAAGTTGTACATG-3' [3'UTR]; when *clec-233* is deleted, the 5' UTR and 3' UTR primers generate a 433-bp PCR product, whereas when WT is present, the 5' UTR and ORF primers generate a 258-bp product) and combination 2 (forward, 5'-CCATGTCAATGTTCTGAGAC-3' [5' UTR]; reverse-1, 5'-GGC GCAGAACTCTTGCTT-3' [ORF]; and reverse-2, 5'-GAGTGAGGA AGTTGTACATG-3' [3'UTR]; deletion, 696 bp; WT, 484 bp).

For genotyping *clec-233(E72A,E73A)*, the following oligos were used for PCR screening: forward, 5'-AGTCATCGTCCGCAGCG-3'; and reverse, 5'-AGGTTATCAGGTTTCGTACG-3'. The presence of mutations E72A and E73A yields a 503-bp band, while lack of mutations yields no band. These mutations were further verified by amplifying the genomic region between oligos 1 (5'-CCATGTCAATGTTCTGAGAC-3') and 2 (5'-AGGTTATCAGGTTTCGTACG-3'), followed by sequencing with oligo 5'-AAGCAA GAGTTTCTGCGCC-3' (sequencing was performed by Retrogen or Eton Bioscience).

Single-copy transgene insertions of *famk-1*

Single-copy transgene insertions were generated using a transposon-based strategy (MosSCI; Frøkjær-Jensen et al., 2008). All *famk-1* transgenes included 2,701 bp upstream of the *famk-1* start codon (*famk-1* promoter) and 1,761 bp downstream of the *famk-1* stop codon (*famk-1* 3' UTR). Both untagged and mCherry/GFP-tagged transgenes were constructed. The different constructs were cloned into vectors with the *Cb-unc-119* selection marker (pCFJ151 for chromosome II [ChrII] insertion [*ttTi5605*] or pCFJ352 for ChrI insertion [*ttTi4348*]) and then injected into strains EG6429 (*ttTi5605*, ChrII) or EG6701 (*ttTi4348*, ChrI) in a mix together with a Mos1 transposase coding plasmid (pJL43.1, *Pglh-2::Mos1* transposase, 50 ng/μl) and three plasmids encoding fluorescent markers for negative selection (pCFJ90 [*Pmyo-2::mCherry*, 2.5 ng/μl], pCFJ104 [*Pmyo-3::mCherry*, 5 ng/μl], and pGH8 [*Prab-3::mCherry*, 10 ng/μl]). After 7–10 d, moving progeny with no fluorescent markers were selected and transgene insertion was confirmed by PCR.

For comparison of WT and D387A mutant of *famk-1*, the coding sequence for mCherry (optimized for expression in *C. elegans*) was inserted at C-terminus immediately before the stop codon (Fig. 1, E and F).

For N-terminal tagging of *famk-1* (Fig. 1, G and H), mCherry sequence was introduced immediately after the signal peptide (i.e., after aa 27) using a synthesized G-block DNA fragment (Integrated DNA Technologies). Two DNA fragments were synthesized then annealed to produce the desired fragment (the sequence was broken into two fragments to break repeats which complicate G-block gene synthesis): fragment 1 (5'-[TGCA-TATCTCCGGTGCCTAACATGCAGTAC]TGGAGTAAATTATTA ATTAATCGCTTTGATCTCTTGTTCCTCATTCTACCCATTA TTTATCTATAATAGCTTATGAACCTCACCCATAAATGCTCA TTTTGCAGTGTACAAAACTGGGAGCCGGGTTTGTGATGAAGC TGAAACCAGCAAAGAGCAAGAAGTGAGACGAGAAAAGTCCAG AAAGACATGCGGTGCAATATAAAGCGATTATTCACCTTTGGCGATC GGAGTTTTTGGCGCTACTGGTTATAATCTCGTTTTCCAAGGGT **GGTGGTGGTGGAGGTTCTGTCTCAAAGGGTGAAGAAGATAAC**

ATGGCAATTATTAAGAGTTTATGCGTTTCAAGGTGCATATG
 GAGGGATCTGTCAATGGGCATGAGTTTAAAATTGAAGGTGAA
 GGAGAAGGCCGACCATATGAGGGAACACAAACCGCAAACTA
 AAGGTAAGTTTAAACATATATACTAACTAACCTGATTAT
 TTAATTTTCAGGTAATAAGGCGGACCATTACCATTGCGCT
GGGACATCCTCT-3') and fragment 2 (5'-GACCATTACCATTCCG
CCTGGGACATCCTCTCTCCACAGTTTATGTATGGAAGTAAAG
 CTTATGTTAAACATCCGGCAGATATACCAGATTATTTGAAAC
 TTTTATTCCCGGAGGGTTTTAAGTGGGAACGCGTAATGAATT
 TTGAAGACGGAGGAGTTGTACAGTGACGCAAGACTCAAGGT
 AAGTTTAAACAGTTCCGTTACTAACTAACCATACATATTTAAA
 TTTTCAGCTCCAAGATGGAGAATTTATTTATAAAGTCAAAC
 TTCGAGGAACGAATTTCCCTCGGATGGACCTGTTATGCAGA
 AGAAGACTATGGGATGGGAAGCTTCAAGTAAAAGAAATGTACC
 CTGAAGACGGTGCTCTTAAGGGAGAGATTAACAACGCTCTTA
 AATTGAAAGATGGAGGACATTACGATGCTGAGGTAAGTTTAA
 ACATGATTTTACTAACTAACTAATCTGATTTAAATTTTCAGG
 TGAAGACAACCTACAAAGCCAAAAAACCAGTTTCAGCTGCCAG
 GAGCGTACAATGTTAATATTAACCTGGATATCACCTCCACA
 ACGAGGATTACACTATCGTTGAGCAATATGAAAGAGCTGAAG
 GGCGGCACTCGACAGGTGGCATGGATGAATTGTATAAGGGA
GGAGGAGGAGGTGGAGACAACTATGAAAGTAAGTTCTAAAAT
 TGTATATGTGTTGTTTATTGGTTGAAAATGATTATTTGAATTCGC
 TAGAAAGGAATAGTGGCGATAGCAATCGATAAAACAAGAGAAAA
 CTATGCCTAAATGTGGCTATAACATGTGGGAGTTTTGTGACAAT
 TTTGT-3'). In both fragments, underlining indicates a 30-bp
 annealing region for the two fragments (within mCherry cod-
 ing sequence); bold indicates a linker consisting of six glycines
 (6xGly linker), positioned before (fragment 1) and after (frag-
 ment 2) the mCherry sequence; and italics indicates a *famk-1*
 sequence between bp 82 and 248. The sequence in brackets
 (fragment 1) is an adapter (designed to increase G/C content for
 G-block synthesis).

The annealed product of the two fragments contains an
 adapter sequence followed by 5' UTR::signal-peptide::6xGly-
 linker::mCherry::6xGly-linker::N-terminus of *famk-1* (bp 82–248).
 The G-block DNA was annealed and amplified using primers
 specific for the 5' and 3' ends and Phusion polymerase (M0530;
 NEB). Gibson assembly (E2611; NEB) was then used to ligate the
 PCR product with WT *famk-1* in vector pOD2230/pAG69, thus
 generating a 5' UTR::signal-peptide::6xGly-linker::mCherry::
 6xGly-linker::*famk-1*::*famk-1*-3'UTR fusion in pOD2318/
 pAG122. mCherry tag was introduced at the same position for
 N-terminal tagging of *famk-1-D387A*, and 5' UTR::signal-pep-
 tide::6xGly-linker::mCherry::6xGly-linker::*famk-1-D387A*::
famk-1-3' UTR fusion was generated (pOD2987).

For expression of ER-retained FAMK-1, a KDEL sequence was
 added at the C-terminus of *famk-1*, right before the STOP codon,
 using the following complementary oligos: forward, 5'-GGATGA
 TAAGAAAAGTGAAGGATGAACTATAGTCTGCATTCGTTAGG
 TCTTC-3'; and reverse, 5'-GAAGACCTAACGAATGACGACTA-
 TAGTTTCATCCTTAACAGTTTTCTTATCATCC-3'. Both oligos
 contain a KDEL coding sequence (underlined), followed by a stop
 codon (bold) and flanked by 19- to 20-bp homology to *famk-1*. For
 comparison of WT and ER-retained FAMK-1, Gibson assembly
 was used (Gibson et al., 2009; cloning kit, E2611; NEB) to insert
 the above KDEL sequence into pOD2318/pAG122 (mCherry::

famk-1), thus generating a transgene encoding mCherry::FAMK-
 1-KDEL (pOD2319/pAG123).

For expression of AMAN-2(aa 1–144) as a spermathecal golgi
 marker (pOD3515/pKL355: *psth-1::aman-2(aa 1–144)::6xGly-link-
 er::mCherry::unc-54-3'UTR*; Fig. S5 B), the *sth-1* promoter was
 used (*psth-1*; Bando et al., 2005). For this, a 1,380-bp region
 upstream of the *sth-1* ORF was amplified with oligos (forward)
 5'-CCGAAAGAACGGCCACAATT-3' and (reverse) 5'-GTTGCT
 CTAGCACAAAAGAC-3'. The *aman-2* sequence (aa 1–144) was
 cloned from genomic DNA with oligos 5'-ATGGGAAAACGCAAT
 TTCTATATTATCC-3' and 5'-CTGCAGGTCTGAATGAGC-3'.

The *mCherry::unc-54 3'UTR* fragment was cloned from
 pCFJ104 (Frøkjær-Jensen et al., 2008).

For spermathecal expression of FAMK-1, the *sth-1* promoter
 (*psth-1*) region as described above was used (*psth-1::his-72*
 [transcriptional reporter, pOD2234/pAG81; Fig. 6 B], *psth-1::
 famk-1* [pOD2240/pAG93; Fig. 6, A and C], or *psth-1::famk-1::gfp*
 [pOD2243/pAG107; Fig. S6 C]). In all constructs, a 1,761-bp region
 of the *famk-1* 3' UTR was used (Fig. 6, A–D; and Fig. S6 C).

Light microscopy

Images in Fig. 2, B and C; Fig. 5, A, B, and D; Fig. 6 B; Fig. S1 B; Fig.
 S2, A–C; Fig. S4 E; Fig. S5, A–C; and Fig. S6 C were acquired on an
 inverted Zeiss Axio Observer Z1 system with a Yokogawa
 spinning-disk confocal head (CSU-X1) and a 63× 1.4-NA Plan
 Apochromat objective (Zeiss). Gravid adult worms were dis-
 sected, and early embryos were collected using mouth pipette.
 Embryos were mounted on a 2% agarose pad in a 5 μl M9 buffer
 and sealed with a #1.5-thickness coverslip. 8 × 1.5-μm z-sections
 were acquired. Images in Fig. 2 C were acquired at 1-min inter-
 vals for 1 h. The environmental temperature during image
 acquisition was typically maintained at 19–20°C, except for ex-
 periments at which the effect of elevated temperature on phe-
 notype was examined, in which environmental temperature was
 maintained at 23°C.

Images of furrow ingression in Fig. S2 A were acquired at 20-s
 intervals. Images in Fig. 4 E and Fig. S3 B were acquired on a
 CV1000 spinning disk confocal system (Yokogawa Electric Cor-
 poration) with a 512 × 512 EM-CCD camera (Hamamatsu), 60×
 1.35-NA U-PlanApo objective and CellVoyager software. Early
 stage embryos were mouth pipetted into wells of a glass-bottom
 384-well Sensoplate (Greiner Bio-One) containing 100 μl of
 0.1 mg/ml tetramisole hydrochloride in M9 (to anesthetize
 worms that later hatch). Before imaging, the plate was spun for
 1 min at 600 ×g to settle the embryos. Images were acquired at
 bright field and two different wavelengths as follows: (1) bright
 field: 90% power, 25 ms, 20% gain; (2) 488 nm: 100% power, 200
 ms, 60% gain; and (3) 568 nm: 45% power, 150 ms, 60% gain. 18 ×
 2-μm z-sections were acquired at 20-min intervals for 10 h.

In Fig. 2 A, to assess the stages of embryonic arrest, the wells
 were postscanned in bright field with a 10× objective 20 h after
 embryos were initially mounted. For imaging germlines in Figs.
 S1 B and S4 E, worms were anesthetized by 20- to 25-min in-
 cubation in a mix of 1 mg/ml Tricaine (ethyl 3-aminobenzoate
 methanesulfonate salt, E10521; Sigma-Aldrich) and 0.1 mg/ml
 tetramisole hydrochloride (T1512; Sigma-Aldrich) in M9 before
 mounting on an agarose pad.

Fertility and embryonic lethality analysis

L4 hermaphrodites were singled on plates at 20°C or 23°C for 24 h (t = 0–24 h). The adult worms were removed to new plates for additional 24-h incubation at the same temperatures (t = 24–48 h). This step was repeated once again (t = 48–72 h). For each set of plates, hatched worms and unhatched embryos (embryonic lethal) were counted ~24 h after the mothers were removed. For the fertility plots, the number of embryos laid during each 24-h interval are presented in Fig. 1, C and F, while in other figures, presented are the sum of embryos laid between 0 and 72 h.

Image acquisition of larval defects

To image worms with morphological larval defects compared with WT N2 (Fig. S1 B), a DinoEye USB eyepiece camera was mounted on a dissection scope and Dino-Lite software was used (Version 1.19.2; AnMo Electronics Corporation). Worms are imaged when moving on the plate.

Spermathecal overexpression of FAMK-1 by extrachromosomal arrays

Gonads of 10 gravid adult worms were injected with a DNA mix consisting of the plasmid coding for FAMK-1::GFP driven by the STH-1 promoter (pOD2243/pAG107, 50 ng/μl) and a plasmid coding for a pharynx fluorescent marker (pCFJ90 [*Pmyo-2::mCherry*], 2.5 ng/μl). 4 d after injection, 15 progeny of generation F1 with apparent pharynx marker (which indicates formation of extrachromosomal arrays) were picked and singled.

After the selected F1 progeny laid eggs, imaging was performed. Plates with F2 progeny to F1 mothers with apparent FAMK-1::GFP in spermatheca (6/15) were maintained. Brood size counts were performed for worms of generation F4, and the expression of spermathecal FAMK-1::GFP was confirmed in these.

FAMK-1 antibody

FAMK-1 (residues 60–512) was expressed using a modified pI-secSUMOstar vector (LifeSensors) and purified from Hi5 insect cells (Bac-to-Bac, B85502; Invitrogen; Xiao et al., 2013). The purified protein was sent to Cocalico Biologicals for immunizing rabbits. FAMK-1-specific antibodies were affinity purified from serum with a HiTrap NHS-activated affinity column (17-0716-01; GE Healthcare) on which FAMK-1 was immobilized.

Immunoblotting

Gravid adult worms were picked, rinsed extensively in M9 buffer, and lysed in Loading Buffer (125 mM Tris, pH 6.8, 10% glycerol, 2% SDS, 0.71 M β-mercaptoethanol, and 0.05% Bromophenol blue). Extracts were separated on SDS-PAGE gels and transferred onto nitrocellulose membranes. Immunoblots were blocked in TBST (10 mM Tris, pH 8.0, 150 mM NaCl, and 0.1% Tween 20) containing 5% milk followed by overnight incubation at 4°C with the affinity-purified anti-FAMK-1 (diluted 1:1,000 in blocking buffer). Immunoblots were washed six times for 5 min each in TBST and incubated with HRP-conjugated anti-rabbit secondary antibody (NA934; GE Healthcare) for 30 min at room temperature. After washing as above, the immunoblots were subjected to chemiluminescent substrates and visualized on film.

In vitro analysis of FAMK-1 substrates

HEK293 cells were grown in DMEM with 10% (vol/vol) fetal bovine serum and 100 μg/ml penicillin/streptomycin (15140-122; GIBCO) at 37°C with 5% CO₂. Cells were transfected using Fugene (E269A; Roche) with potential FAMK-1 substrates harboring C-terminal V5-His tags (WT or EE>AA mutants) and either WT or kinase-defective (D387A) FAMK-1 with a C-terminal FLAG tag. Plasmids used for in vitro analysis of FAMK-1 substrates are listed in Table S3.

After recovery for 24 h, cells were extensively rinsed with TBS and ³²P-labeled for 6–12 h in media consisting of phosphate-free DMEM, 10% FBS (dialyzed), and 0.5 mCi orthophosphate. The cell extracts and media were then harvested for immunoprecipitation. For experiments in which FAMK-1-FLAG::KDEL was cotransfected with Clec-233 V5-His, the cells were treated as described above, except labeling was performed in serum-free phosphate-free DMEM containing 0.5 mCi orthophosphate.

Cell extract immunoprecipitation of FLAG-tagged FAMK-1. Cells were rinsed with TBS and lysed in 400 μl 50 mM Tris, pH 8.0, 150 mM NaCl, 1.0% NP-40 (vol/vol), 10% glycerol, and 0.4 mM EDTA (modified RIPA buffer) containing protease inhibitors and phosphatase inhibitors. The lysate was cleared by centrifugation at 18,000 ×g for 10 min at 4°C. Protein concentration was determined, and equal amounts of protein were added to protein gel loading buffer (extract sample). The remaining extract was precleared using ~30 μl protein G-beads (20397; Thermo Fisher Scientific) and incubated with agitation for 15 min at 4°C. The beads were pelleted, and the extract was subjected to immunoprecipitation using 25 μl mouse anti-FLAG M2 affinity resin (A2220; Sigma-Aldrich). After incubation with agitation at 4°C overnight, the beads were pelleted followed by washing six times with modified RIPA buffer. The extract sample or FLAG immunoprecipitation from the extract was used in all cases to confirm expression of the transfected construct encoding FAMK-1. To determine the extent of FAMK-1 secretion, FLAG immunoprecipitation of the medium was performed as follows. The medium (5 ml) was precleared by centrifugation at 1,000 ×g for 10 min. The supernatant was removed and treated as described above for the cell extract FLAG immunoprecipitations.

Media immunoprecipitation of V5-tagged lectins. Cell debris was removed by centrifugation at 1,000 ×g for 10 min and the media supernatant then precleared by the addition of protein G-beads as above. After removal of the beads, the media was immunoprecipitated using 1 μl rabbit anti-V5 antibody (AB3792; Millipore) and 25 μl protein-G beads rocked at 4°C overnight. The beads were collected and washed as described for the FLAG immunoprecipitations. The V5 immunoprecipitates were analyzed by immunoblotting and autoradiography.

For CLEC-110, which was not secreted efficiently into the medium, V5 immunoprecipitation from cell extracts was necessary; in this case, the extract was first used for immunoprecipitation with rabbit anti-V5 antibody and then immunoprecipitated as above using anti-FLAG M2.

Phylogenetic analysis

Amino acid sequences of the FAMK-1 orthologues were aligned using Clustal O (Sievers et al., 2011), and the tree was generated using phylo dendron software.

Calcium signaling in the spermatheca during embryo transits

Image acquisition. Eggs were obtained by dissolving gravid hermaphrodites in a solution of sodium hydroxide and sodium hypochlorite followed by three washes with M9. Drops of M9 containing eggs were plated onto nematode growth medium plates seeded with *Escherichia coli* OP50, and incubated at 20°C for 68 h. Animals close to their first ovulation were selected for imaging, anaesthetized with 0.01% tetramisole and 0.1% tricaine in M9 buffer, and mounted on 2% agarose pads.

Images were acquired on a Nikon Eclipse 80i microscope using a 60× 1.40-NA objective. Fluorescence was monitored using a standard GFP filter set (excitation 470/40, beam splitter 495, emission 525/50; Chroma Technology), with fluorescence excitation provided by a Nikon Intensilight C-HGFI 130-W mercury lamp, attenuated at the source with the ND16 neutral density filter, and shuttered between exposures using a Smart-Shutter (Sutter Instruments) triggered by the camera transistor-transistor logic signal.

Images were captured using a SPOT RT3 monochrome CCD camera, and acquisitions were controlled by SPOT Advanced 5 software (Diagnostic Instruments). Images were acquired at a rate of one frame per second, an exposure time of 75 ms, and a gain of 8. The full chip of the camera was used, generating images 1,600 × 1,200 pixels in size. Time-lapse image sequences were saved as 8-bit TIF files.

Image processing. All image processing was done using Fiji (<http://fiji.sc/>). Each time-lapse image sequence was registered to a single frame, rotated to put the spermatheca in a standard orientation, and cropped to a standard size of 800 × 400 pixels (100 μm × 50 μm). Following this standardization step, GCaMP time series values (F) were generated for each frame of the image sequence by calculating the mean pixel intensity (total pixel intensity/area). For each time series, the baseline GCaMP value (F₀) was obtained by averaging the 30 frames before oocyte entry, and the normalized GCaMP time series (F/F₀) was calculated by dividing the entire GCaMP time series by the baseline GCaMP value. Normalized GCaMP time series are shown plotted in GraphPad Prism (GraphPad Software).

Heat maps of multiple GCaMP time series were generated using MATLAB (The MathWorks). Each time series was cropped to start at the 50th frame before oocyte entry and was appended with zeros until the length matched the longest time series in the set. The time series were then assembled into a matrix where each row is a different time series and time increases with the columns. This matrix was then displayed as an image, and the color map was scaled so all heat maps were displaying the same range.

DIC imaging of spermathecae

For the experiment in Fig. 6 C, half-moon-stage L4 larvae were transferred to plates freshly seeded with OP50 and incubated at 20°C for 24, 48, or 72 h. Animals were mounted on 2% agarose in 0.1 M sodium azide and observed immediately with DIC microscopy to score gonad phenotypes.

Online supplemental material

Fig. S1 shows schematics of the generation of *famk-1Δ* and *famk-1* single-copy transgenes and images of phenotypes observed in

famk-1Δ. Fig. S2 shows analysis of cytokinetic furrow ingression in *famk-1Δ* and images of localization of NMY-2 and HMR-1 in *famk-1Δ*. Fig. S3 shows DLG-1 localization in *famk-1Δ* and analysis of *famk-1Δ* fertility. Fig. S4 shows analysis of lectins as putative substrates of FAMK-1. Fig. S5 shows analysis of WT and KDEL mCherry::FAMK-1 localization and FAMK-1 colocalization with a Golgi marker in spermatheca. Fig. S6 shows analysis of spermatheca-expressed FAMK-1. Table S1 lists hits from proteome-wide “SSSEE” motif search, which are predicted to also have a signal peptide and/or transmembrane domains. Table S2 lists strains used in the study. Table S3 lists plasmids used for analysis of FAMK-1 substrate phosphorylation. Video 1 shows an example of partition loss between adjacent cells leading to multinucleation in a *famk-1Δ* embryo.

Acknowledgments

We thank members of the Dixon, Desai, and Oegema laboratories for helpful discussions, Coleman Clifford for technical support, and Vincent Tagliabracchi and Shirin Bahmanyar for their input during the initial stages of the project.

Some *C. elegans* strains were provided by the Caenorhabditis Genetics Center, which is funded by the National Institutes of Health Office of Research Infrastructure Programs (P40 OD010440). This work was supported by the National Institutes of Health (grants DK018849-41 and DK018024043 to J.E. Dixon and C.A. Worby, grant GM074215 to A. Desai, and grant GM110268 to E.J. Cram). A. Gerson-Gurwitz was supported by an European Molecular Biology Organization long-term fellowship (ALTF 251-2012). A. Desai and K. Oegema acknowledge salary and other support from the Ludwig Institute for Cancer Research.

The authors declare no competing financial interests.

Author contributions: A. Gerson-Gurwitz, C.A. Worby, J.E. Dixon, K. Oegema, and A. Desai initiated the project; A. Gerson-Gurwitz, C.A. Worby, and K-Y. Lee performed the majority of experiments; R. Khaliullin contributed to imaging and image analysis; J. Bouffard and E.J. Cram performed analysis of spermathecal calcium signaling and morphology; D. Cheerambathur contributed to strain generation; and A. Gerson-Gurwitz, C.A. Worby, J.E. Dixon, and A. Desai prepared the manuscript, with input from all other authors.

Submitted: 6 July 2018

Revised: 11 July 2019

Accepted: 25 August 2019

References

- Arribere, J.A., R.T. Bell, B.X. Fu, K.L. Artilles, P.S. Hartman, and A.Z. Fire. 2014. Efficient marker-free recovery of custom genetic modifications with CRISPR/Cas9 in *Caenorhabditis elegans*. *Genetics*. 198:837–846. <https://doi.org/10.1534/genetics.114.169730>
- Bahl, J.M., S.S. Jensen, M.R. Larsen, and N.H. Heegaard. 2008. Characterization of the human cerebrospinal fluid phosphoproteome by titanium dioxide affinity chromatography and mass spectrometry. *Anal. Chem.* 80:6308–6316. <https://doi.org/10.1021/ac800835y>
- Bando, T., T. Ikeda, and H. Kagawa. 2005. The homeoproteins MAB-18 and CEH-14 insulate the dauer collagen gene col-43 from activation by the

- adjacent promoter of the Spermatheca gene *sth-1* in *Caenorhabditis elegans*. *J. Mol. Biol.* 348:101–112. <https://doi.org/10.1016/j.jmb.2005.01.045>
- Bies, C., C.M. Lehr, and J.F. Woodley. 2004. Lectin-mediated drug targeting: history and applications. *Adv. Drug Deliv. Rev.* 56:425–435. <https://doi.org/10.1016/j.addr.2003.10.030>
- Brown, G.D., J.A. Willment, and L. Whitehead. 2018. C-type lectins in immunity and homeostasis. *Nat. Rev. Immunol.* 18:374–389. <https://doi.org/10.1038/s41577-018-0004-8>
- Byerly, L., R.C. Cassada, and R.L. Russell. 1976. The life cycle of the nematode *Caenorhabditis elegans*. I. Wild-type growth and reproduction. *Dev. Biol.* 51:23–33. [https://doi.org/10.1016/0012-1606\(76\)90119-6](https://doi.org/10.1016/0012-1606(76)90119-6)
- Cancino, J., A. Capalbo, A. Di Campi, M. Giannotta, R. Rizzo, J.E. Jung, R. Di Martino, M. Persico, P. Heinklein, M. Salles, and A. Luini. 2014. Control systems of membrane transport at the interface between the endoplasmic reticulum and the Golgi. *Dev. Cell.* 30:280–294. <https://doi.org/10.1016/j.devcel.2014.06.018>
- Carrascal, M., M. Gay, D. Ovelheiro, V. Casas, E. Gelpí, and J. Abian. 2010. Characterization of the human plasma phosphoproteome using linear ion trap mass spectrometry and multiple search engines. *J. Proteome Res.* 9:876–884. <https://doi.org/10.1021/pr900780s>
- Cui, J., J. Xiao, V.S. Tagliabracchi, J. Wen, M. Rahdar, and J.E. Dixon. 2015. A secretory kinase complex regulates extracellular protein phosphorylation. *eLife.* 4:e06120. <https://doi.org/10.7554/eLife.06120>
- Fradin, M., C. Stoetzel, J. Muller, M. Koob, D. Christmann, C. Debry, M. Kohler, M. Isnard, D. Astruc, P. Desprez, et al. 2011. Osteosclerotic bone dysplasia in siblings with a *Fam20C* mutation. *Clin. Genet.* 80:177–183. <https://doi.org/10.1111/j.1399-0004.2010.01516.x>
- Frøkjær-Jensen, C., M.W. Davis, C.E. Hopkins, B.J. Newman, J.M. Thummel, S.P. Olesen, M. Grunnet, and E.M. Jørgensen. 2008. Single-copy insertion of transgenes in *Caenorhabditis elegans*. *Nat. Genet.* 40:1375–1383. <https://doi.org/10.1038/ng.248>
- Gerald, N., J. Dai, H.P. Ting-Beall, and A. De Lozanne. 1998. A role for Dicotylostelium *racE* in cortical tension and cleavage furrow progression. *J. Cell Biol.* 141:483–492. <https://doi.org/10.1083/jcb.141.2.483>
- Ghazarian, H., B. Itoni, and S.B. Oppenheimer. 2011. A glycobiology review: carbohydrates, lectins and implications in cancer therapeutics. *Acta Histochem.* 113:236–247. <https://doi.org/10.1016/j.acthis.2010.02.004>
- Gibson, D.G., L. Young, R.Y. Chuang, J.C. Venter, C.A. Hutchison III, and H.O. Smith. 2009. Enzymatic assembly of DNA molecules up to several hundred kilobases. *Nat. Methods.* 6:343–345. <https://doi.org/10.1038/nmeth.1318>
- Gorelik, E., U. Galili, and A. Raz. 2001. On the role of cell surface carbohydrates and their binding proteins (lectins) in tumor metastasis. *Cancer Metastasis Rev.* 20:245–277. <https://doi.org/10.1023/A:1015535427597>
- Green, R.A., H.L. Kao, A. Audhya, S. Arur, J.R. Mayers, H.N. Fridolfsson, M. Schulman, S. Schloissnig, S. Niessen, K. Laband, et al. 2011. A high-resolution *C. elegans* essential gene network based on phenotypic profiling of a complex tissue. *Cell.* 145:470–482. <https://doi.org/10.1016/j.cell.2011.03.037>
- Ishikawa, H.O., A. Xu, E. Ogura, G. Manning, and K.D. Irvine. 2012. The Raine syndrome protein *FAM20C* is a Golgi kinase that phosphorylates biomineralization proteins. *PLoS One.* 7:e42988. <https://doi.org/10.1371/journal.pone.0042988>
- Johnson, S.A., and T. Hunter. 2005. Kinomics: methods for deciphering the kinome. *Nat. Methods.* 2:17–25. <https://doi.org/10.1038/nmeth731>
- Kamath, R.S., A.G. Fraser, Y. Dong, G. Poulain, R. Durbin, M. Gotta, A. Kanapin, N. Le Bot, S. Moreno, M. Sohrmann, et al. 2003. Systematic functional analysis of the *Caenorhabditis elegans* genome using RNAi. *Nature.* 421:231–237. <https://doi.org/10.1038/nature01278>
- Kim, H., T. Ishidate, K.S. Ghanta, M. Seth, D. Conte Jr., M. Shirayama, and C.C. Mello. 2014. A co-CRISPR strategy for efficient genome editing in *Caenorhabditis elegans*. *Genetics.* 197:1069–1080. <https://doi.org/10.1534/genetics.114.166389>
- Kimble, J., and D. Hirsh. 1979. The postembryonic cell lineages of the hermaphrodite and male gonads in *Caenorhabditis elegans*. *Dev. Biol.* 70:396–417. [https://doi.org/10.1016/0012-1606\(79\)90035-6](https://doi.org/10.1016/0012-1606(79)90035-6)
- Koike, T., T. Izumikawa, J. Tamura, and H. Kitagawa. 2009. *FAM20B* is a kinase that phosphorylates xylose in the glycosaminoglycan-protein linkage region. *Biochem. J.* 421:157–162. <https://doi.org/10.1042/BJ20090474>
- Koob, M., B. Doray, M. Fradin, D. Astruc, and J.L. Dietemann. 2011. Raine syndrome: expanding the radiological spectrum. *Pediatr. Radiol.* 41:389–393. <https://doi.org/10.1007/s00247-010-1875-4>
- Köppen, M., J.S. Simske, P.A. Sims, B.L. Firestein, D.H. Hall, A.D. Radice, C. Rongo, and J.D. Hardin. 2001. Cooperative regulation of *AJM-1* controls junctional integrity in *Caenorhabditis elegans* epithelia. *Nat. Cell Biol.* 3:983–991. <https://doi.org/10.1038/ncb1101-983>
- Kovacevic, I., J.M. Orozco, and E.J. Cram. 2013. Filamin and phospholipase C-ε are required for calcium signaling in the *Caenorhabditis elegans* spermatheca. *PLoS Genet.* 9:e1003510. <https://doi.org/10.1371/journal.pgen.1003510>
- Leiser, S.F., A. Begun, and M. Kaeberlein. 2011. HIF-1 modulates longevity and healthspan in a temperature-dependent manner. *Aging Cell.* 10:318–326. <https://doi.org/10.1111/j.1474-9726.2011.00672.x>
- Leiser, S.F., G. Jafari, M. Primitivo, G.L. Sutphin, J. Dong, A. Leonard, M. Fletcher, and M. Kaeberlein. 2016. Age-associated vulval integrity is an important marker of nematode healthspan. *Age (Dordr.)* 38:419–431. <https://doi.org/10.1007/s11357-016-9936-8>
- Levin, M., T. Hashimshony, F. Wagner, and I. Yanai. 2012. Developmental milestones punctuate gene expression in the *Caenorhabditis elegans* embryo. *Dev. Cell.* 22:1101–1108. <https://doi.org/10.1016/j.devcel.2012.04.004>
- Lindberg, I., H.W. Pang, J.P. Stains, D. Clark, A.J. Yang, L. Bonewald, and K.Z. Li. 2015. FGF23 is endogenously phosphorylated in bone cells. *J. Bone Miner. Res.* 30:449–454. <https://doi.org/10.1002/jbmr.2354>
- Mann, K., and F. Siedler. 2006. Amino acid sequences and phosphorylation sites of emu and rhea eggshell C-type lectin-like proteins. *Comp. Biochem. Physiol. B Biochem. Mol. Biol.* 143:160–170. <https://doi.org/10.1016/j.cbpb.2005.11.003>
- Manning, G., D.B. Whyte, R. Martinez, T. Hunter, and S. Sudarsanam. 2002. The protein kinase complement of the human genome. *Science.* 298:1912–1934. <https://doi.org/10.1126/science.1075762>
- Minko, T. 2004. Drug targeting to the colon with lectins and neoglycoconjugates. *Adv. Drug Deliv. Rev.* 56:491–509. <https://doi.org/10.1016/j.addr.2003.10.017>
- Mody, R., S. Joshi, and W. Chaney. 1995. Use of lectins as diagnostic and therapeutic tools for cancer. *J. Pharmacol. Toxicol. Methods.* 33:1–10. [https://doi.org/10.1016/1056-8719\(94\)00052-6](https://doi.org/10.1016/1056-8719(94)00052-6)
- Nakamura, A., C. Ly, M. Cipetić, N.A. Sims, J. Vieusseux, V. Kartsogiannis, S. Bourallexis, H. Saleh, H. Zhou, J.T. Price, et al. 2007. Osteoclast inhibitory lectin (OCIL) inhibits osteoblast differentiation and function in vitro. *Bone.* 40:305–315. <https://doi.org/10.1016/j.bone.2006.09.001>
- Paschinger, K., M. Hackl, M. Guttermigg, D. Kretschmer-Lubich, U. Stemmer, V. Jantsch, G. Lochnit, and I.B. Wilson. 2006. A deletion in the golgi alpha-mannosidase II gene of *Caenorhabditis elegans* results in unexpected non-wild-type N-glycan structures. *J. Biol. Chem.* 281:28265–28277. <https://doi.org/10.1074/jbc.M602878200>
- Petrella, L.N. 2014. Natural variants of *C. elegans* demonstrate defects in both sperm function and oogenesis at elevated temperatures. *PLoS One.* 9:e112377. <https://doi.org/10.1371/journal.pone.0112377>
- Pollak, A.J., K. Haghghi, S. Kunduri, D.A. Arvanitis, P.A. Bidwell, G.S. Liu, V.P. Singh, D.J. Gonzalez, D. Sanoudou, S.E. Wiley, et al. 2017. Phosphorylation of serine96 of histidine-rich calcium-binding protein by the *Fam20C* kinase functions to prevent cardiac arrhythmia. *Proc. Natl. Acad. Sci. USA.* 114:9098–9103. <https://doi.org/10.1073/pnas.1706441114>
- Pollard, T.D. 2007. Regulation of actin filament assembly by Arp2/3 complex and formins. *Annu. Rev. Biophys. Biomol. Struct.* 36:451–477. <https://doi.org/10.1146/annurev.biophys.35.040405.101936>
- Pulvirenti, T., M. Giannotta, M. Capestrano, M. Capitani, A. Pisanu, R.S. Polishchuk, E. San Pietro, G.V. Beznoussenko, A.A. Mironov, G. Turacchio, et al. 2008. A traffic-activated Golgi-based signalling circuit coordinates the secretory pathway. *Nat. Cell Biol.* 10:912–922. <https://doi.org/10.1038/ncb1751>
- Raine, J., R.M. Winter, A. Davey, and S.M. Tucker. 1989. Unknown syndrome: microcephaly, hypoplastic nose, exophthalmos, gum hyperplasia, cleft palate, low set ears, and osteosclerosis. *J. Med. Genet.* 26:786–788. <https://doi.org/10.1136/jmg.26.12.786>
- Reinhart, B.J., F.J. Slack, M. Basson, A.E. Pasquinelli, J.C. Bettinger, A.E. Rougvie, H.R. Horvitz, and G. Ruvkun. 2000. The 21-nucleotide *let-7* RNA regulates developmental timing in *Caenorhabditis elegans*. *Nature.* 403:901–906. <https://doi.org/10.1038/35002607>
- Rolls, M.M., D.H. Hall, M. Victor, E.H. Stelzer, and T.A. Rapoport. 2002. Targeting of rough endoplasmic reticulum membrane proteins and ribosomes in invertebrate neurons. *Mol. Biol. Cell.* 13:1778–1791. <https://doi.org/10.1091/mbc.01-10-0514>
- Salvi, M., L. Cesaro, E. Tibaldi, and L.A. Pinna. 2010. Motif analysis of phosphosites discloses a potential prominent role of the Golgi casein kinase (GCK) in the generation of human plasma phospho-proteome. *J. Proteome Res.* 9:3335–3338. <https://doi.org/10.1021/pr100058r>

- Sievers, F., A. Wilm, D. Dineen, T.J. Gibson, K. Karplus, W. Li, R. Lopez, H. McWilliam, M. Remmert, J. Söding, et al. 2011. Fast, scalable generation of high-quality protein multiple sequence alignments using Clustal Omega. *Mol. Syst. Biol.* 7:539. <https://doi.org/10.1038/msb.2011.75>
- Simpson, M.A., R. Hsu, L.S. Keir, J. Hao, G. Sivapalan, L.M. Ernst, E.H. Zackai, L.I. Al-Gazali, G. Hulskamp, H.M. Kingston, et al. 2007. Mutations in FAM20C are associated with lethal osteosclerotic bone dysplasia (Raine syndrome), highlighting a crucial molecule in bone development. *Am. J. Hum. Genet.* 81:906–912. <https://doi.org/10.1086/522240>
- Sreelatha, A., L.N. Kinch, and V.S. Tagliabracci. 2015. The secretory pathway kinases. *Biochim. Biophys. Acta.* 1854:1687–1693. <https://doi.org/10.1016/j.bbapap.2015.03.015>
- Tagliabracci, V.S., J.L. Engel, J. Wen, S.E. Wiley, C.A. Worby, L.N. Kinch, J. Xiao, N.V. Grishin, and J.E. Dixon. 2012. Secreted kinase phosphorylates extracellular proteins that regulate biomineralization. *Science.* 336:1150–1153. <https://doi.org/10.1126/science.1217817>
- Tagliabracci, V.S., L.A. Pinna, and J.E. Dixon. 2013. Secreted protein kinases. *Trends Biochem. Sci.* 38:121–130. <https://doi.org/10.1016/j.tibs.2012.11.008>
- Tagliabracci, V.S., S.E. Wiley, X. Guo, L.N. Kinch, E. Durrant, J. Wen, J. Xiao, J. Cui, K.B. Nguyen, J.L. Engel, et al. 2015. A Single Kinase Generates the Majority of the Secreted Phosphoproteome. *Cell.* 161:1619–1632. <https://doi.org/10.1016/j.cell.2015.05.028>
- Takeuchi, T., R. Sennari, K. Sugiura, H. Tateno, J. Hirabayashi, and K. Kasai. 2008. A C-type lectin of *Caenorhabditis elegans*: its sugar-binding property revealed by glycoconjugate microarray analysis. *Biochem. Biophys. Res. Commun.* 377:303–306. <https://doi.org/10.1016/j.bbrc.2008.10.001>
- Tseng, Y., and D. Wirtz. 2004. Dendritic branching and homogenization of actin networks mediated by arp2/3 complex. *Phys. Rev. Lett.* 93:258104. <https://doi.org/10.1103/PhysRevLett.93.258104>
- Vogel, P., G.M. Hansen, R.W. Read, R.B. Vance, M. Thiel, J. Liu, T.J. Wronski, D.D. Smith, S. Jeter-Jones, and R. Brommage. 2012. Ameiogenesis imperfecta and other biomineralization defects in *Fam20a* and *Fam20c* null mice. *Vet. Pathol.* 49:998–1017. <https://doi.org/10.1177/0300985812453177>
- Wang, X., J. Hao, Y. Xie, Y. Sun, B. Hernandez, A.K. Yamoah, M. Prasad, Q. Zhu, J.Q. Feng, and C. Qin. 2010. Expression of FAM20C in the osteogenesis and odontogenesis of mouse. *J. Histochem. Cytochem.* 58:957–967. <https://doi.org/10.1369/jhc.2010.956565>
- Ward, S., and J.S. Carrel. 1979. Fertilization and sperm competition in the nematode *Caenorhabditis elegans*. *Dev. Biol.* 73:304–321. [https://doi.org/10.1016/0012-1606\(79\)90069-1](https://doi.org/10.1016/0012-1606(79)90069-1)
- Wen, J., J. Xiao, M. Rahdar, B.P. Choudhury, J. Cui, G.S. Taylor, J.D. Esko, and J.E. Dixon. 2014. Xylose phosphorylation functions as a molecular switch to regulate proteoglycan biosynthesis. *Proc. Natl. Acad. Sci. USA.* 111:15723–15728. <https://doi.org/10.1073/pnas.1417993111>
- Wewer, U.M., K. Ibaraki, P. Schjørring, M.E. Durkin, M.F. Young, and R. Albrechtsen. 1994. A potential role for tetranectin in mineralization during osteogenesis. *J. Cell Biol.* 127:1767–1775. <https://doi.org/10.1083/jcb.127.6.1767>
- Xiao, J., V.S. Tagliabracci, J. Wen, S.A. Kim, and J.E. Dixon. 2013. Crystal structure of the Golgi casein kinase. *Proc. Natl. Acad. Sci. USA.* 110:10574–10579. <https://doi.org/10.1073/pnas.1309211110>
- Yue, R., B. Shen, and S.J. Morrison. 2016. Clec11a/osteolectin is an osteogenic growth factor that promotes the maintenance of the adult skeleton. *eLife.* 5:e18782. <https://doi.org/10.7554/eLife.18782>
- Zhang, H., Q. Zhu, J. Cui, Y. Wang, M.J. Chen, X. Guo, V.S. Tagliabracci, J.E. Dixon, and J. Xiao. 2018. Structure and evolution of the *Fam20* kinases. *Nat. Commun.* 9:1218. <https://doi.org/10.1038/s41467-018-03615-z>
- Zhou, H., V. Kartsogiannis, J.M. Quinn, C. Ly, C. Gange, J. Elliott, K.W. Ng, and M.T. Gillespie. 2002. Osteoclast inhibitory lectin, a family of new osteoclast inhibitors. *J. Biol. Chem.* 277:48808–48815. <https://doi.org/10.1074/jbc.M209059200>
- Zhou, W., M.M. Ross, A. Tessitore, D. Ornstein, A. Vanmeter, L.A. Liotta, and E.F. Petricoin III. 2009. An initial characterization of the serum phosphoproteome. *J. Proteome Res.* 8:5523–5531. <https://doi.org/10.1021/pr900603n>